MICROCHEMICAL CHARACTERIZATION OF ASH FROM FUEL PRODUCTION

by

Melissa Kay Brock

Thesis submitted to the Faculty of the

Virginia Polytechnic Institute and State University

in partial fulfillment of the requirements for the degree of

MASTER OF SCIENCE

in

Geology

APPROVED:

J. R. Craig, Chairman

J. D. Rimstidt

S. J. DeCanio

July, 1993

Blacksburg, Virginia

MICROCHEMICAL CHARACTERIZATION OF ASH FROM FUEL PRODUCTION

by

Melissa Kay Brock

Committee Chairman: James R. Craig
Geological Sciences

(ABSTRACT)

Millions of tons of ash and slag are produced each year as a result of energy production. This study looks at the mineralogy and textures in the ash resulting from the gasification of a 25% Passaic Valley sewage sludge, 75% Pittsburgh #8 coal slurry in a Texaco gasification facility and at ash resulting from the incineration of municipal solid waste at several facilities in Virginia and North Carolina. This information is then compared with similar studies done on ash and slag from coal-burning power plants and a study done on petroleum coke slag which was produced at a Texaco gasification facility. Lastly, a comparison of bulk chemistries of ashes to those of soil and crustal rocks is made. A general understanding of the stability of elements, especially metals, in terms of the phases in which they are contained as well as the textures, was hoped to be gained from this study.

Samples for this study were polished sections which were 2.54 cm in diameter that were set in cold-setting epoxy then ground and polished. Samples were then studied under a reflected light microscope before being carbon coated for study on a SEM and an electron microprobe. Photos of textures and analyses were made throughout.

At least 50% of the ash from all sources was a Si-Al oxide rich glass which had varying amounts of Fe, Ca, K, P, Mg, and Ti and other trace elements. Fe oxides and spinels were common phases found. Pb and Zn were rarely encountered, but were found as both oxides and sulfides. Cr was found in the form of spinels, often covered by a protective Al enriched outer rim. The heavy metals found were successfully bound as mineral analogs or as a glass phase. The only phase found to be reactive was an AlC matrix containing subhedral SiC crystals. The Al phase effervesced when placed in contact

with water, changing from tan to green/blue/violet in color, releasing a gas (probably CO_2, C_2H_2, or CH_4) in the process.

ACKNOWLEDGEMENTS

My first thanks goes to my parents, Barbara Brock and Jack McNeil, for putting up with me for six years at a college that was only an hour from a home-cooked meal. Mom, so this is what I can do with rocks when I grow up! I would also like to thank my grandmothers, both of whom were always nearby if I needed to escape from school. Special thanks goes to my grandfather, now deceased, who convinced me with stories from WW II that maybe college wasn't that bad and that I shouldn't drop out.

The chairman of my committee, Jim Craig, has been a great help and a priceless friend. When I finished my B.S. here, Dr. Craig helped me obtain a fellowship from Texaco to get my M.S. Even though he has been Department Chairman and serves on endless committees, he has always had time to read through yet another draft of my thesis. Thanks for understanding my rescue squad endeavors. Don Rimstidt has also always been there to help with any puzzle I come across and actually seems to look forward to reading rough drafts of this thesis. Thanks to Steve DeCanio for being my Texaco link, showing me what a gasifier is and to Todd Solberg who has provided essential technical expertise on the electron microprobe and the SEM.

Thanks to all of the numerous grad students who through my years here have been great. For anything from how to get things centered using an Apple computer (I grew up on IBM) to how to use the SEM, they are always eager to pass on what they have learned. They aren't too bad at hacky sack either, although we did get some strange looks in Mexico.

I am very grateful to Texaco for supporting me with a generous fellowship for the past two years. Having to only work on my own project allowed me some extra time to grow and get involved with the community volunteering with Blacksburg and Roanoke rescue squads. Thanks to all of the people at Texaco who have come to Virginia Tech to talk about my project and to those who continue to send me information related to my project that has been released by Texaco.

Thanks also to the Department of the Interior's Mineral Institutes program administered by the Bureau of Mines under allotment grant number G1184151 for support at Virginia Tech.

TABLE OF CONTENTS

LIST OF FIGURES

LIST OF TABLES

Microchemical Characterization of Ash From Fuel Production

Introduction and Scope of Study

Energy production by means of fossil fuels, sludge, and municipal solid waste combustion produces millions of tons of ash per year. These ashes are composed of the non-flammable and non-volatile constituents which have become concentrated by at least one order of magnitude and then fused into glasses or synthetic analogs of minerals. Heretofore, these ashes have generally been considered as another waste, albeit now in a more compact and less odoriferous form. The great variability no doubt leads to significant heterogeneity, but there have been few studies which examined the nature of the ash. In recent years, increased concerns about waste disposal, in general, and ash disposal in particular, have brought to focus the need for careful assessment of these materials. Their proper disposal, if only a waste, and potential use, if essentially benign, can only be addressed if physical and chemical characteristics have been examined and evaluated.

This study was designed to examine and characterize specifically sludge gasification ash and municipal waste incinerator ash and to compare them with similar ash generated by the combustion of coal and petroleum coke. The characterization concentrated on identifying, analyzing, and examining the textures of the phases present within the ashes. Many of the phases were expected to be synthetic analogs of minerals because the bulk chemistry of many ash samples is similar to those of igneous rocks and the conditions of formation also parallel some geologic processes. Special attention was paid to textures in the sludge and municipal waste ashes, which were preserved during sample preparation, and which might give clues to how different metals are bound in the system. In a parallel study, Carl Kirby has examined different aspects of municipal waste incinerator ash including leachabilities of various salts and heavy metals and has investigated ways to identify mineral analogs using x-ray diffraction (XRD).

The terms "slag", "ash", and "deposit" have been rather indiscriminately used when referring to the solid by-products of gasification and incineration although no significant difference has generally been implied by these terms. In the present work, "slag" will generally refer to the coarser glassy material, whereas "ash" will refer to the finer grained particles. The term "deposit" will be used for the material that has solidified on some part of the processing plant itself. The terms are not intended to imply any significant difference

in origin or composition.

Samples

There were basically two types of samples studied for this project. The first type, with which the first portion of this thesis deals, are samples of ash/slag generated at Texaco's Montebello research gasification facility in California by burning of a slurry composed of 25% Passaic Valley sewage sludge and 75% Pittsburgh #8 coal. The second type of sample is ash/slag generated by the incineration of municipal solid waste from various facilities in Virginia and North Carolina. Both types of samples were treated the same way for analysis.

Sample Preparation

Most samples were prepared as polished sections which were 1 cm thick and 2.54 cm in diameter. The ash/slag material was cut to fit plastic molds using a water cooled saw. Once dried, the samples were placed in the molds, and were encapsulated in cold-setting epoxy which hardened in 8-10 hours. Samples which were porous or fissile were vacuum impregnated. Once hardened, samples were ground on metal-bonded diamond laps of 600 and 1200 grit with water, and then polished on one micron alpha-alumina or diamond paste on glass using water as a lubricant. At this point, samples were examined under the reflected light microscope. Before analysis on the SEM and microprobe, the samples were carbon coated to reduce charging effects during analysis.

Instrumental Technique

Reflected-light microscope:

The ash and slag samples were examined under the reflected light microscope at different magnifications, noting areas of possible metallic concentrations as well as textures. Pictures were taken of high-interest areas to aid in locating them on the SEM and to document textures. Most glass and several oxide phases exhibited low reflectivities (<10%) whereas the native metal phases had reflectance (R%) values of 50% or greater; the spinel phases present in many samples had R% values similar to those of natural spinels (R~20%) using standard techniques as described in Craig and Vaughan (1981).

Scanning Electron Microscope:

After optical examination, samples were analyzed using a Camscan II scanning electron microscope equipped with an *hnu* System 5000 energy dispersive system. Samples were examined and analyzed with a working distance of 26-35 mm, an accelerating voltage of 20 kv, an emission setting of 1.2, a resolution setting of 3, and a beam current of approximately 1.9 nanoamperes. A live time of 30 seconds was used for analysis and *hnu* software was used to compute weight percent and atomic percent of the elements found, using a standardless analysis option titled "bulk zap". This provided quantitative to semi-quantitative analysis. This analysis routine always sums results to 100 percent; repeated comparison of analyses with results from the electron microprobe demonstrate that the data are accurate $\pm$ 1 percent.

Electron Microprobe:

Quantitative chemical analysis was carried out using a Cameca SX 50 electron microprobe. Analytical conditions were always kept at an acceleration voltage of 15-20 kv, using a series of four PET and LiF crystals appropriately adjusted for the elements in the sample for detection. Geological standards were used.

Sludge Ash Studies

Mode of Generation:

Sludge ash studied was produced during gasification of a 75% Pittsburgh #8 coal, 25% Passaic Valley, New Jersey, sewage sludge (PVSS) slurry by means of the Texaco Gasification Process. In this process, the slurry is reacted with a limited amount of oxygen using an entrained bed gasifier which has a concurrent flow of oxygen and feed. These are reacted at 350-900 psi and temperatures above the melting point of the ash in the feed stream (>2200^{o}F or 1200^{o}C) in the slagging mode for maximum energy production, with the beneficial side effect of destroying undesirable hydrocarbons. This results in the production of "syngas", a mixture of hydrogen and carbon monoxide which is marketed for use as a feedstock for chemical production or as a clean burning fuel for power generation. Up to 99% of the sulfur is removed during the process to produce a marketable elemental sulfur. (Zang and Kahn, 1991)

A by-product produced by the concentration of non-volatile constituents in the gasifier is a slag/ash which is the subject of this study. Ash and slag were studied from

different points in the gasification process. Figure 1 illustrates the basic plant layout with corresponding sample numbers next to the areas from which they were taken.

Bulk Chemistry and Concentration Factors:

Overall, bulk chemistries are dominated by Si-Al-Fe-Ca oxides, which make up approximately 90% of the ash in the form of a glass. Concentrations of Ti, Cr, Zn, and Pb can be found in certain parts of the system, while Ba levels tend to remain low but fairly constant. The heavy metals are present primarily in the slag but are also found on the small concentrations of deposit materials formed during gasification. These deposits are in the form of scales which often flake off of the surface. See Table 1 for the detailed bulk chemistries of the different samples. Discussion of bulk chemistries of the samples follows below in the order in which the samples are generated in the gasifier system.

Bulk chemical analysis of sample #1 shows that a majority of the components are Si, Al, Fe, and Ca oxides. While this analysis also shows trace amounts of the heavy metals Zn, Pb, Cr, and Ba, none were found during SEM analysis.

Results of a Texaco chemical analysis from SEM-EDS studies of both the inner and outer scales of sample #2 (burner face deposit) are in Table 1 where they have been converted to oxides. These results show the inner scale to be composed predominantly of Pb, Si, Zn, and Al oxides, whereas the outer scale contains high quantities of Zn and Si possibly due to temperature differences.

Bulk chemical analysis shows that a majority of sample #3 (cooling coil deposit) is composed of Si, Al, Fe, and Ca, with Pb and Zn levels elevated above those in the feed stock, probably because these volatile metals condense on the cooler surface when they, in some vapor form, come in contact with it.

No bulk analysis of sample #4 of the throat region was available; however, SEM analysis shows much of the sample to be composed of Si, Al, Ca, Fe, K, and Cr oxides.

Bulk chemical analysis of sample # 5 shows that the most abundant components at this stage of the process are Si, Al, Fe, and Ca oxides, very similar to sample #1; however the Fe has been concentrated by a factor of two.

No bulk chemical analysis of sample #6 was available, although it would probably be very similar to that of sample #5 because they are both samples of the coarse slag.

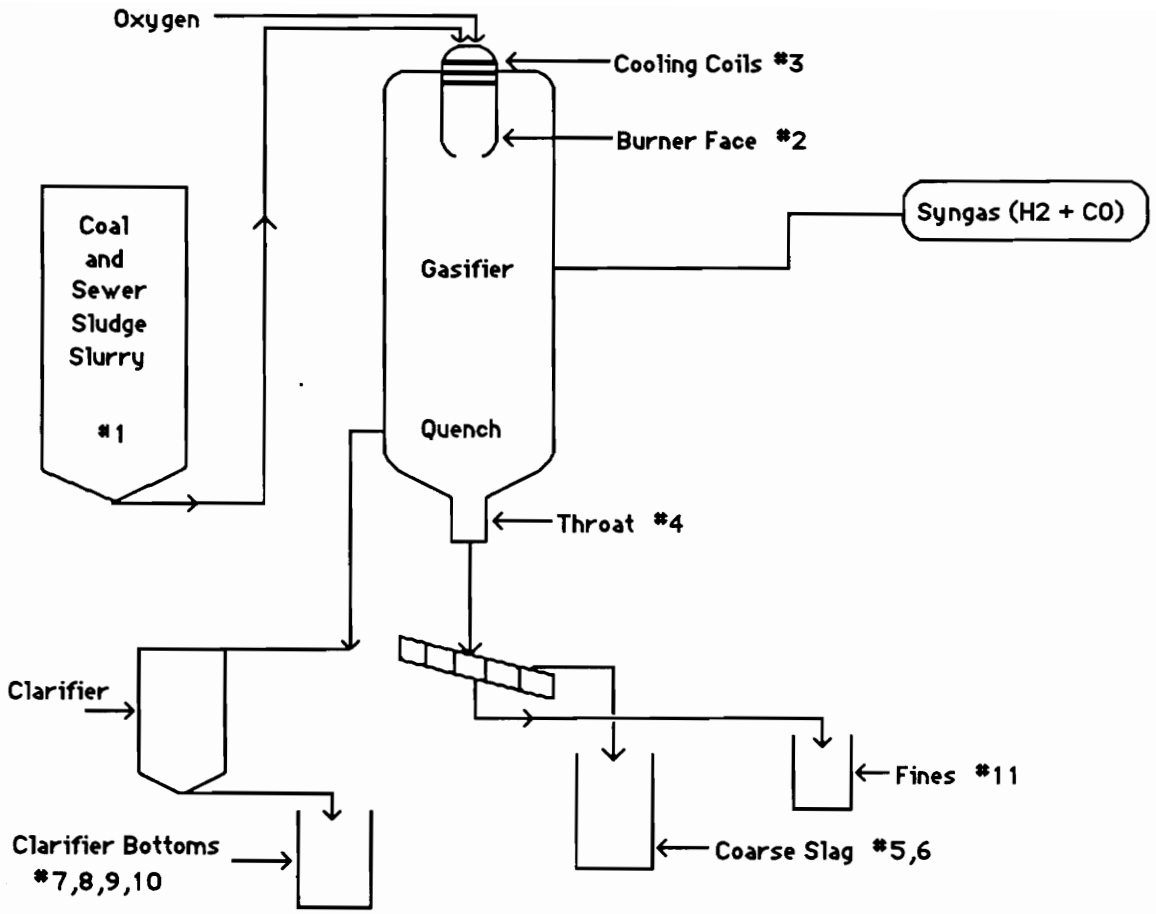

Figure 1. Schematic diagram of the Texaco Gasification Process. Numbers correspond to sample numbers.

Table 1. Bulk chemical analyses of several Texaco samples. Results are in weight percent oxides. (Data provided by Texaco.)

Component	Sample #1	Inner Scale Sample #2	Outer Scale Sample #2	Sample #3	Sample #5
SiO_2	43.15	11.84	9.89	43.90	46.05
Al_2O_3	22.12	9.29	8.28	22.84	21.74
Fe_2O_3	9.76	3.74	8.15	11.71	16.15
CaO	8.94	0.83	0.76	6.92	7.72
MgO	1.87	0.17	----	1.56	1.54
Na_2O	0.73	----	----	0.98	0.88
K_2O	1.29	0.82	1.28	1.09	1.68
TiO_2	2.54	0.28	0.25	2.03	1.76
P_2O_5	2.70	7.88	12.72	2.79	1.52
MnO	0.13	----	----	0.09	0.10
Cr_2O_3	0.06	----	----	0.22	0.30
ZnO	0.33	13.63	45.26	1.51	0.07
PbO	0.22	51.52	13.02	1.95	0.10
BaO	0.10	----	----	0.14	0.11
CuO	0.14	----	----	0.17	0.12
NiO	----	----	0.39	0.07	0.09
SrO	0.08	----	----	0.10	0.09
Totals	94.16	100.00	100.00	98.07	100.02

Phases and Mineral Analogs:

Most of each sample is composed of glass; however, analogs to mineral phases (see Table 2) were found to occur in varying quantities in slags from all parts of the system. Spinel structure minerals, $M_X^{2+}W_2^{3+}Z_4^{2-}$ with Cr-Fe-Al as the major cations were abundant in sample #4 and #11, pyrrhotite ($Fe_{1-x}S$) was found in sample #'s 1,4,6 and 9-11, and sphalerite (ZnS), pyrite (FeS_2), and galena (PbS) equivalents were found in sample #2 and #3. Table 2 is a chart showing the presence or absence of different mineral analogs in the different samples as well as changes in glass compositions throughout the system. Tables 1-11 in Appendix A list glass compositions determined by SEM for each sample.

The following sample descriptions are given in the order in which the samples appear in the gasifier system. **Sample #1** is a dried sample of the feed stock composed of the PVSS and coal. SEM analysis shows most of the detectable grains to be composed of predominantly clays with minor amounts of pyrite, apatite, quartz, an iron oxide, and a probable amphibole of grunerite composition. Coal macerals cannot be analyzed on the SEM because of their low atomic weight. Trace amounts of Ti were found throughout the clays.

Sample #2 is a scale deposit on the burner face composed of two distinct regions -- the inner and outer scales. SEM analysis shows the majority of the sample to be composed of a Si-Al oxide glass and a Si-Fe-Al-Ca oxide glass within which were small porous patches of Si-Al-Zn and Zn-Si-Al-P rich areas, the second with up to approximately 17 weight percent Pb. While some of the Zn has probably formed ZnS, there is not enough sulfur present for all of the Zn and Pb to form sulfides. Zn tends to form sulfides at lower sulfur activities than does Pb, therefore all of the Pb and most of the Zn have probably formed as oxides. Trace amounts of Ti are found throughout the glasses. Copper was also found in one spot which was also rich in iron and aluminum.

Sample #3 is a light scale from the cooling coil which is exposed, at least part of the time, to gas flow within the gasifier. SEM analysis shows most of the grains to be composed of a predominantly Si-Al-Fe oxide glass. Some grains have skeletal sphalerite crystals 5-10 microns in size with as much as 20% of the Zn being substituted by Fe (see Figure 2). Some areas also have skeletal Fe-Al spinels (see Figure 3), which are 1-8 microns in size. Some areas within the sample which appear to be clumps of ash stuck together contain some particles which are galena (PbS) (brightest) and other specks of ZnS

Table 2. Phases and mineral analogs in the different Texaco samples, as well as changes in glass compositions throughout the system. The bottom portion of the chart summarizes the types of textural features observed in the samples. M=Major, m=minor, and t=trace.

Phases	**Mineral**	**Sample Numbers**										
	Analogs	**1**	**2**	**3**	**4**	**5**	**6**	**7**	**8**	**9**	**10**	**11**
SiO_2	Quartz	M	--	--	--	--	--	--	--	--	--	--
$FeSiO_3$	Grunerite	m	--	--	--	--	--	--	--	--	--	--
FeS_2	Pyrite	m	--	--	--	--	--	--	--	--	--	--
Fe	Iron	--	--	--	--	t	--	--	--	--	t	t
$Fe_{1-x}S$	Pyrrhotite	m	--	--	--	--	m	--	m	--	m	m
Fe_2S		--	--	--	--	--	--	--	M	t	M	--
Fe_2S+Fe		--	--	--	--	--	--	t	--	M	--	m
Fe oxide		t	--	--	--	m	--	--	--	--	--	--
(Zn,Fe)S	Sphalerite	--	t	m	--	--	t	--	t	--	--	--
ZnO		--	t	--	--	--	--	--	--	--	--	t
Cr-Al-Fe spinel		--	--	--	M	--	M	--	--	--	--	t
Fe-Al spinel		--	--	m	--	--	--	--	--	--	--	--
PbS	Galena	--	t	t	--	--	--	--	--	--	t	--
PbO		--	t	--	--	--	--	--	--	--	--	--
CuS		--	--	--	--	t	--	--	--	--	--	--
$Ca_5(PO_4)_3$	Apatite	t	--	--	--	--	--	--	--	--	t	--
	Clays	M	--	--	--	--	--	--	--	--	--	--
Glasses:												
Si-Al oxide		--	--	--	--	--	--	--	--	--	--	m
Si-Al-Fe oxide		--	--	m	--	--	--	--	--	--	--	--
Si-P-Al oxide		--	m	--	--	--	--	--	--	--	--	--
Si-Al-Ca oxide		--	m	--	--	--	--	--	--	--	--	--
Si-Al-Fe-Ca oxide		--	M	--	M	M	M	M	M	M	M	M
Textures:												
Skeletal spinels		--	--	--	X	--	--	--	--	--	--	X

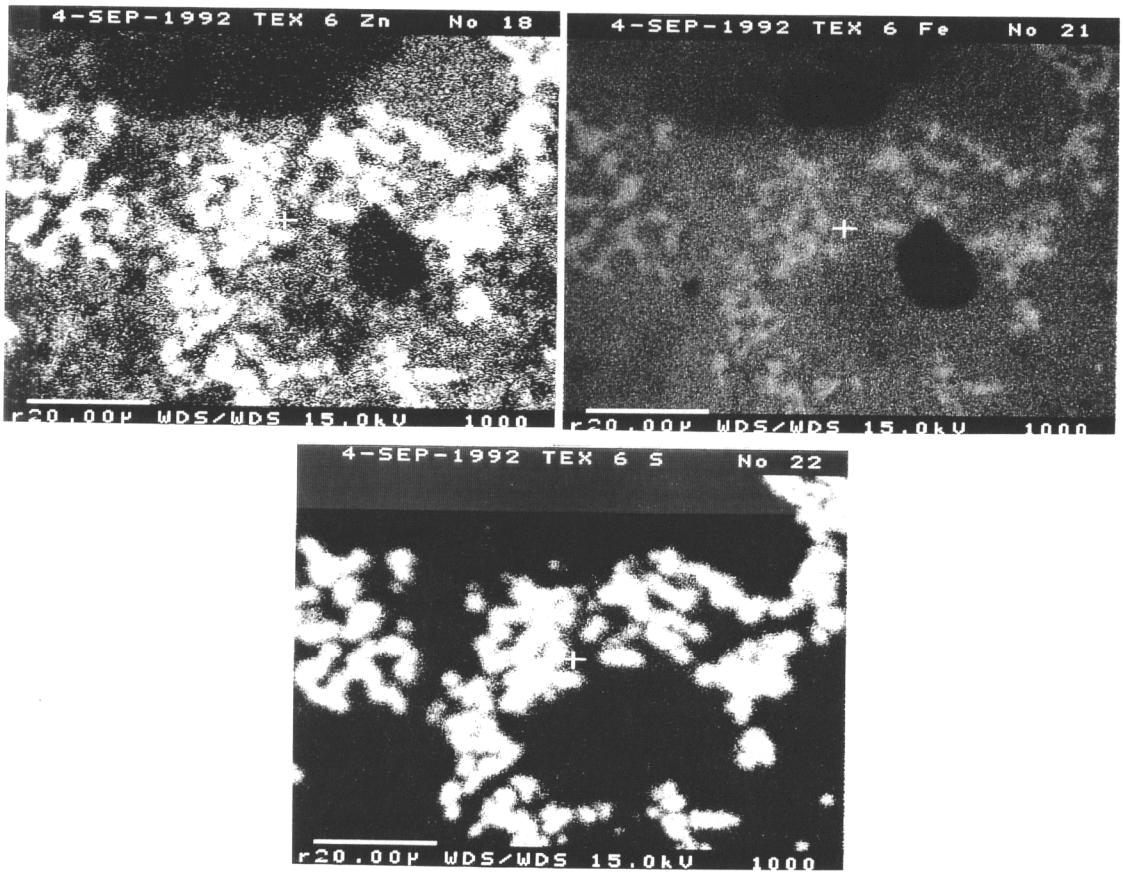

Figure 2. Zn, Fe, and S x-ray maps of Sample #3 generated on the microprobe showing the Fe-rich nature of the sphalerite (ZnS).

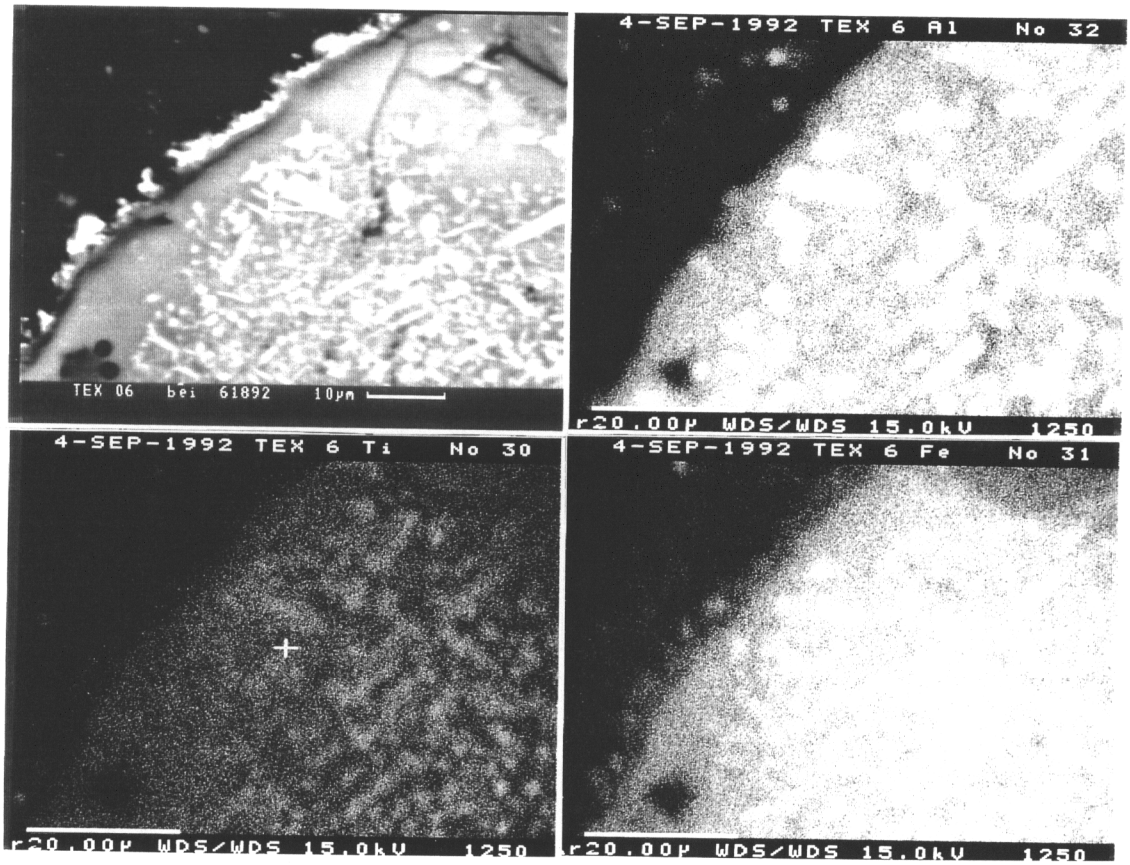

Figure 3. Images of a grain in Sample #3. Photo A is an SEM backscattered electron image of the region shown in Photos B, C, and D along the boundary of a spherical grain containing skeletal Fe-Al-Ti spinels. Photos B-D are x-ray maps generated by the microprobe.

(medium bright) as can be seen in Figure 4, a backscattered electron image (bei). Trace amounts of Ti were found throughout the sample. All ZnS grains were found to contain some Fe substituting for Zn (see Table 3, Appendix A for actual data).

Sample #4 is from a throat scale. Molten slag drops down and begins cooling as it passes through the throat of the gasifier, located at the base of the unit. The groundmass of sample #4 was composed of a Si-Al-Ca-Fe oxide glass, with minor amounts of K. Multiple cruciform crystals of Cr-Al-Fe spinels , a few of which had less than 1 atomic percent Mn, are found throughout the glass (see Figure 5). Figure 6 is a bar graph illustrating the compositions of the spinels (1-8) versus that of the groundmass (9) (see Table 4B, Appendix A has the actual weight percent data). No Ti was found within this sample.

Sample #5 is coarse slag left over from the process. SEM analysis showed most of the grains to be composed of a Si-Al-Fe-Ca oxide glass. A few small grains were composed almost entirely of Fe oxide with minor Cr and less than 1 weight percent S. One grain inspected had a skeletal copper sulfide growing on its surface (see Figure 7). Trace amounts of Ti were found in only the glass grains.

Sample #6 is also coarse slag from the quench left over from the process, similar to sample #5. Like sample #5, this sample was mainly composed of Si-Al-Fe-Ca oxide rich glass. Most grains had at least one "droplet" of $Fe_{1-x}S$ (see Figure 8) or Cr-Fe-Al spinel (see Figure 9), but no Ti or free Fe was found in this sample.

Sample #'s 7-10 are all clarifier bottoms (solids that settle out of the quench water); however, each one was cooled under different conditions to see which condition was best to prevent PbS and ZnS from oxidizing. **Sample #7** was taken out of the clarifier at 170°F (~77°C) and cooled to 90°F (~32°C) under a N_2 blanket. SEM analysis showed the majority of the grains to be mostly composed of a Si-Al-Fe-Ca oxide glass. One fragment which may be a chip off of the refractory brick, approximately 100 microns across, was about 60 weight percent Cr oxide, the remainder being composed of Si, Fe, S, and Al oxides. Another fragment was found that was almost pure Fe (<5 weight percent S). No Ti was found in sample #7. Note that Pb and Zn were only found at concentrations near the level of detection. See Figure 10 of one graph showing general SEM data on several grains examined as well as the photo with the corresponding grains (see Table 7B, Appendix A for numerical data).

Sample #8 was removed from the clarifier at 170°F and cooled to 49°F (~9.4°C)

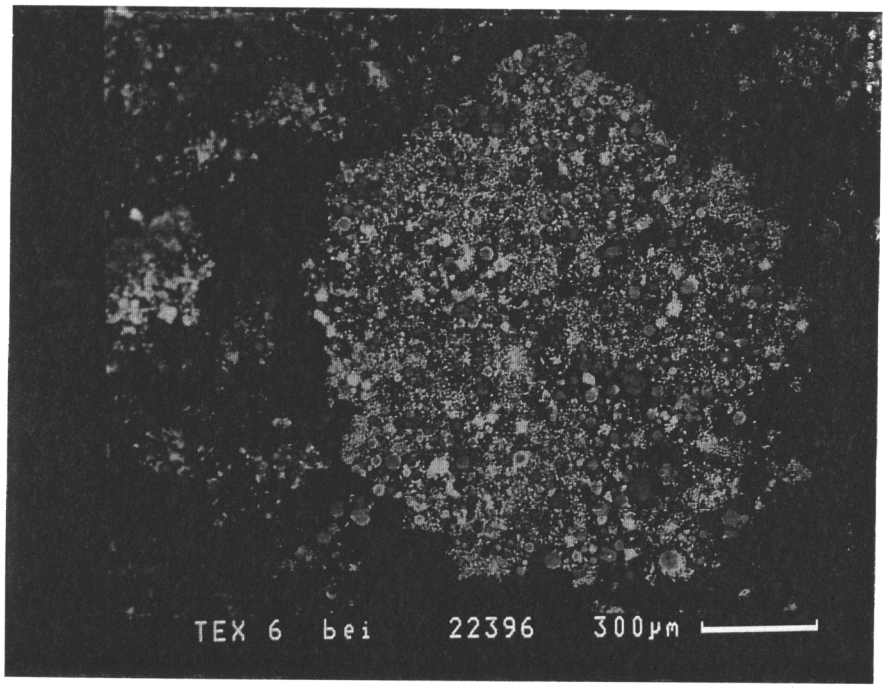

Figure 4. SEM backscattered electron image showing the nature of some of the "grains" in Sample #3 when the ash clumps together.

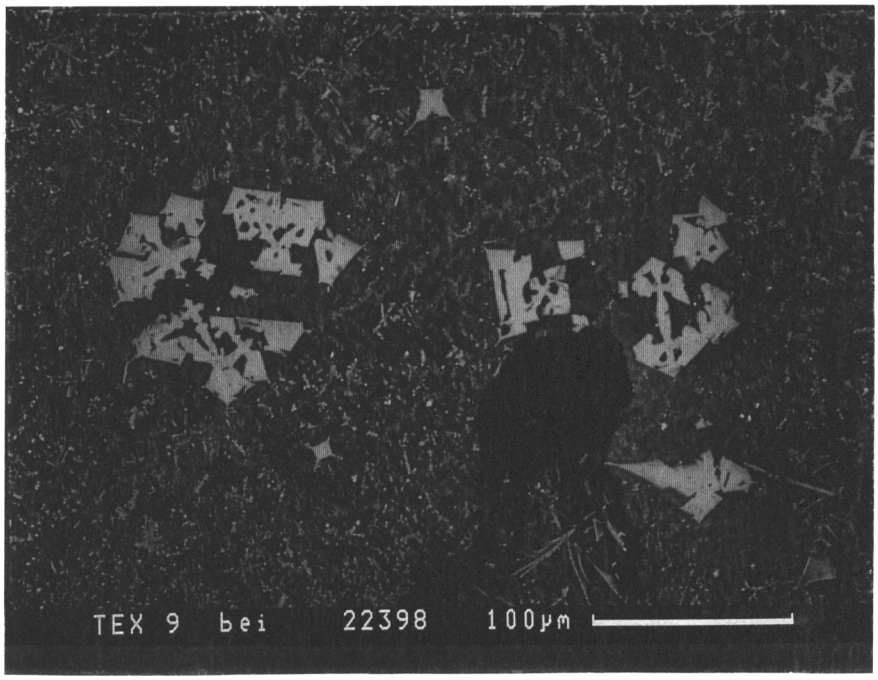

Figure 5. SEM backscattered electron image of cruciform Cr-Al-Fe spinels in Sample #4 from the throat region of the gasifier.

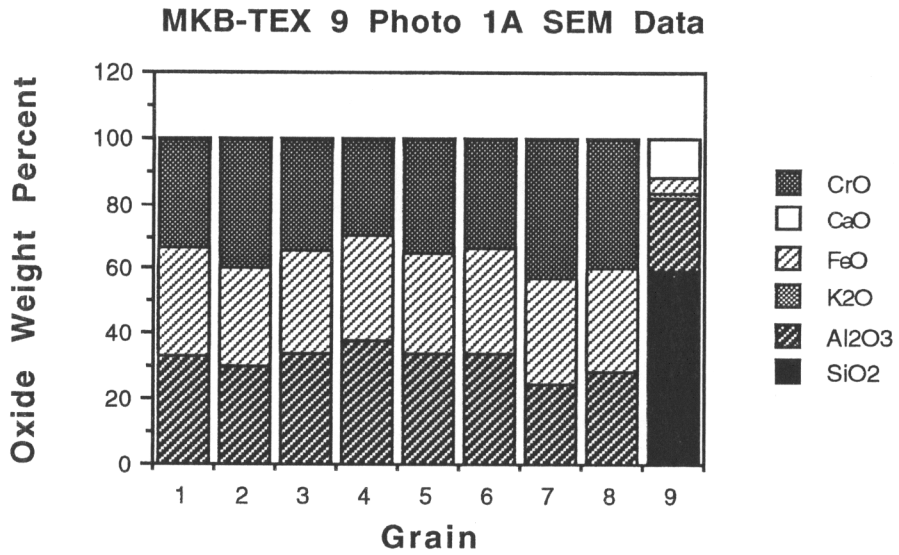

Figure 6. Bar graph illustrating the compositions of several spinels (1-8) versus that of the groundmass (9) in Sample #4.

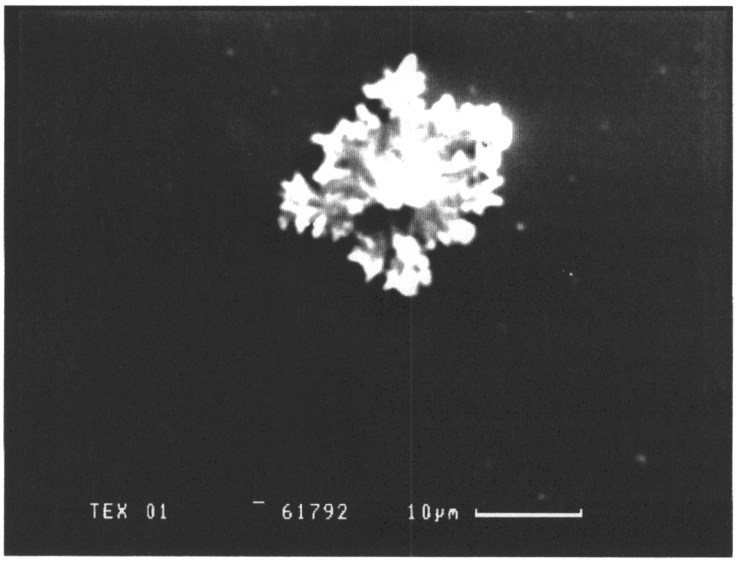

Figure 7. SEM secondary electron image of a skeletal copper sulfide growing on the surface of Sample #5 (a coarse slag sample).

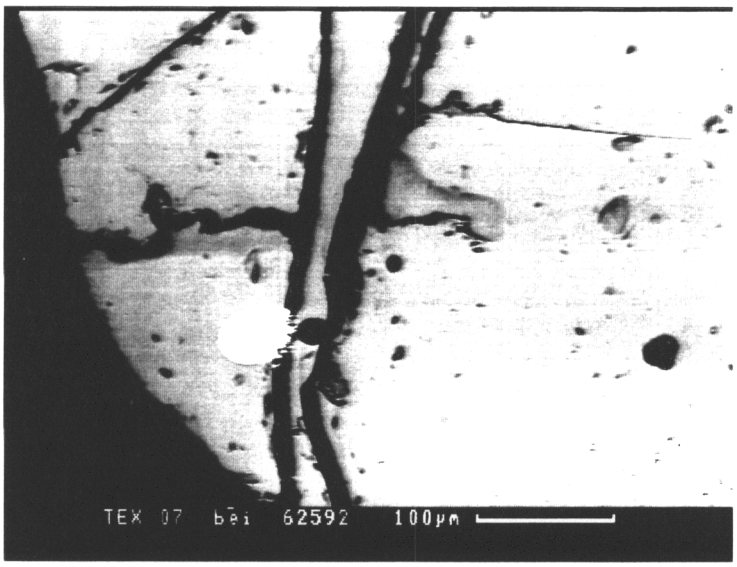

Figure 8. SEM backscattered electron image showing a typical pyrrhotite ($Fe_{1-x}S$) droplet in a glassy matrix found in Sample #6 (a coarse slag sample).

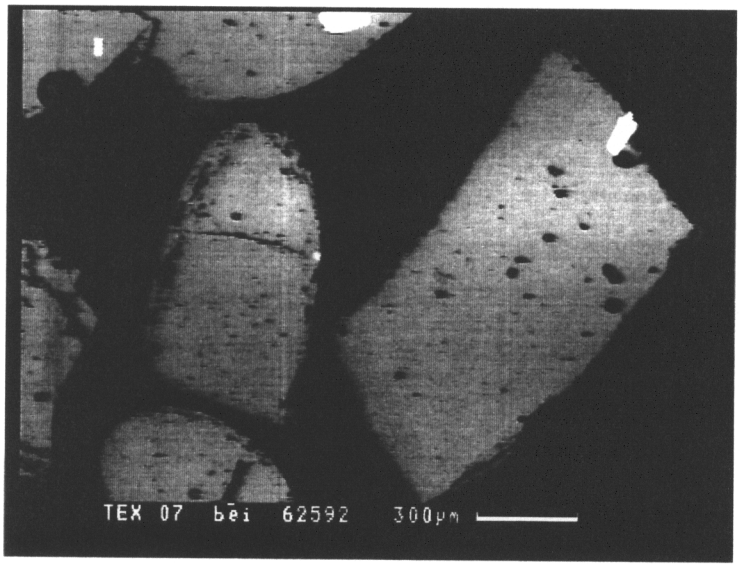

Figure 9. SEM backscattered electron image showing bright regions of Cr-Fe-Al spinel found in the matrix of Sample #6.

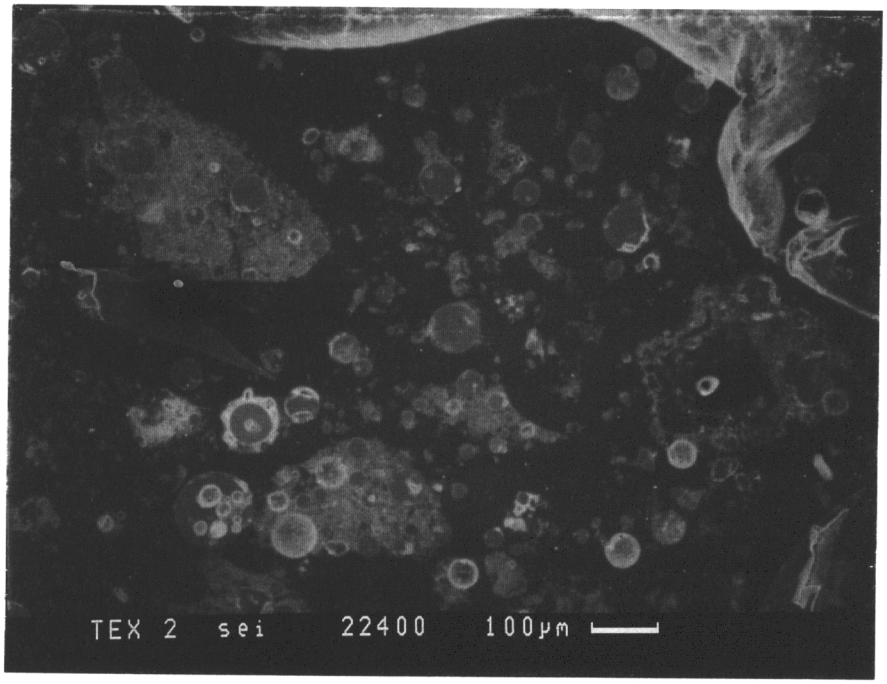

Figure 10.A. SEM secondary electron image of a portion of Sample #7 (clarifier bottoms). Numbers on grains correspond to grain numbers on graph in Figure 10. B.

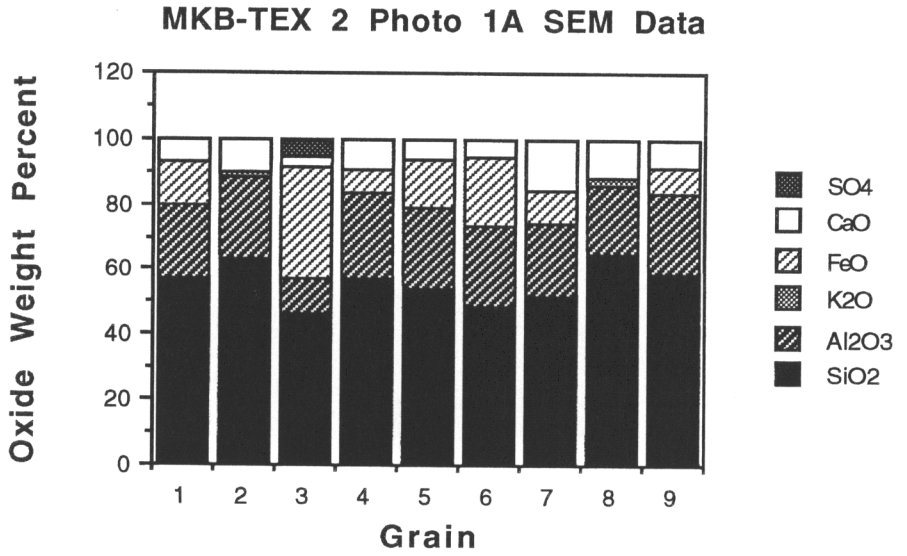

Figure 10. B. SEM data on various grains in Sample #7. Grain numbers at the bottom of the graph correspond to grain numbers in Figure 10. A.

under N_2 before being exposed to normal air. SEM analysis shows most of these grains to be composed of a Si-Al-Fe-Ca oxide glass. This sample, like sample #7, is composed of very porous grains which look like dust particles glued together as can be seen in Figure 11. The brightest areas in Figure 11 are $Fe_{1-x}S$ while the fine grained "groundmass" at one point was 13 weight percent Zn with inadequate quantities of S to make ZnS, suggesting that some of the ZnS has been oxidized; however, analysis of another area in the groundmass sufficient quantities of S to form ZnS. Analysis of several metallic grains yielded bulk compositions of approximately Fe_2S; these appear to be submicroscopic intergrowths of Fe and FeS near the composition of the eutectic between these phases. Trace amounts of Ti were found within the glass.

Sample #'s 9 and 10 were both taken out of the clarifier at 170°F and were not cooled under a N_2 blanket, but were instead only cooled in contact with normal air. Similar to the other clarifier samples, the bulk of these samples was composed of a Si-Al-Fe-Ca oxide glass. Several grains in both samples had regions of FeS and Fe intergrown on a microscale as noted above. No Pb or Zn was found in sample #9; however, one fragment found in sample #10 illustrated definite zoning of elements, including Pb and Zn (see Figure 12) with results similar to those for the outer scale of the burner face deposit from where it might have broken off . SEM data of the area in sample #10 yielded too little S for all of the Pb to be tied up as PbS. Trace amounts of Ti was found in the glass in both samples. Figure 13 shows a graph of SEM data for some areas in sample #9 (see Table 9B, Appendix A for SEM data).

The last sample in the process is **sample #11**, the lock hopper fines (fine slag). Similar to the clarifier bottoms, SEM analysis shows the majority of this material to be a Si-Al-Fe-Ca oxide glass. Minor amounts of $Fe_{1-x}S$ and Fe were found as "droplets" within some of the glass grains. One fragment containing skeletal Fe-Cr-Al oxide spinel was found, probably chipped off of the refractory brick within the gasifier. See Figure 14 for a typical picture of the material in Sample #11. Ti was found in trace amounts in most grains except for those high in Fe.

Textures:

Samples display a wide variety of textures on both the micro- and megascales. Although glasses dominate, crystalline phases are present as primary euhedral crystals and as exsolution phases as skeletal and cruciform crystals. Dendritic spinels occur in several

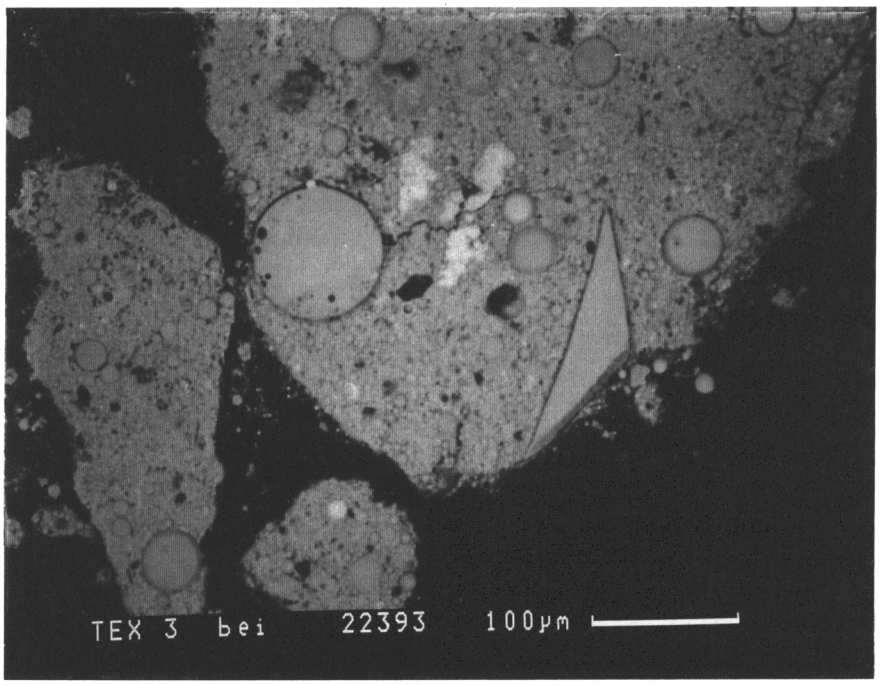

Figure 11. SEM backscattered electron image illustrating the porous nature of Sample #8 (clarifier bottoms). Brightest areas are of $Fe_{1-x}S$.

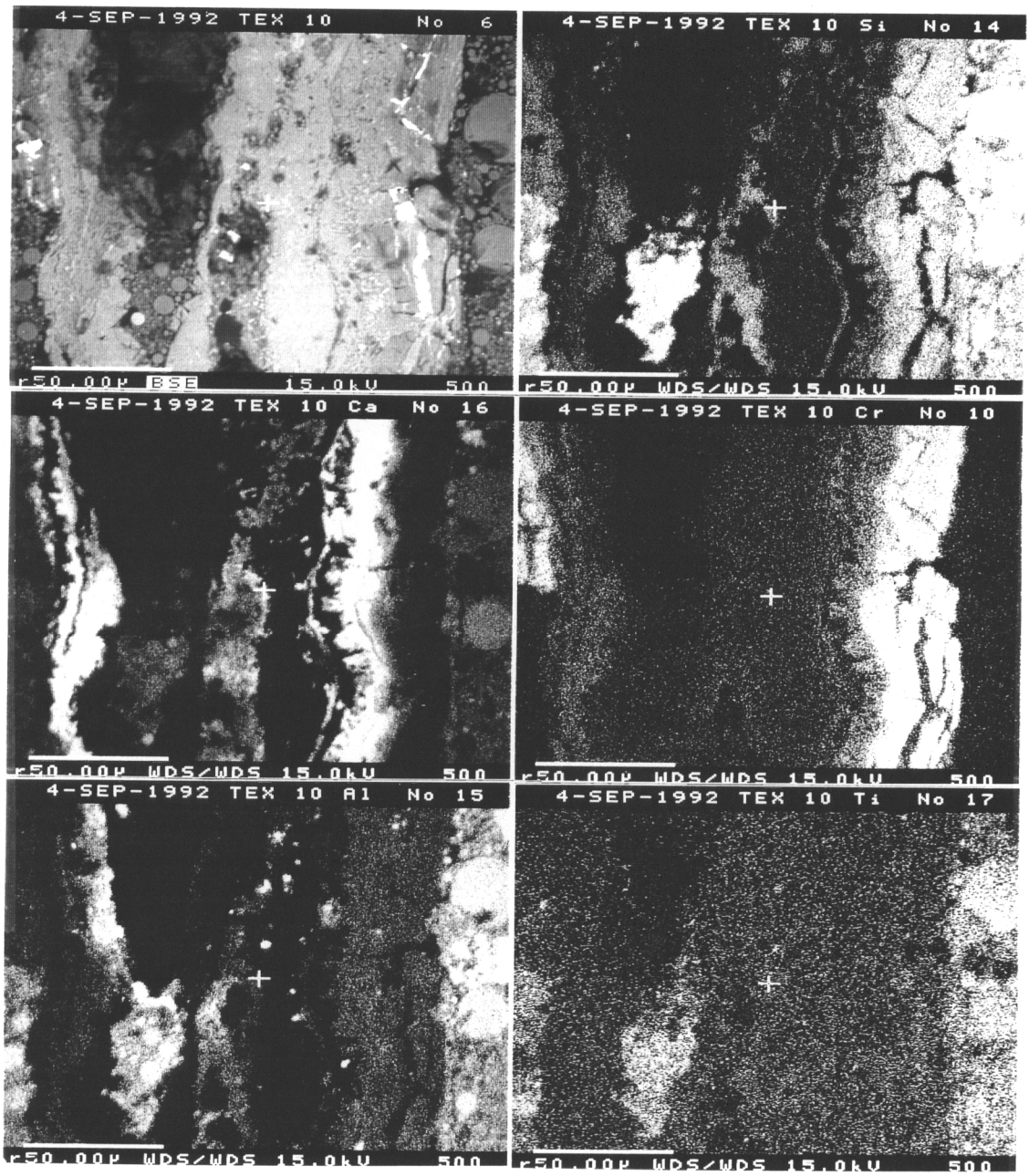

Figure 12. Photos of the clarifier bottom Sample #10. Top left photo is a microprobe backscattered electron image of a zoned grain. The other photos are x-ray maps generated by the microprobe. (More photos next page)

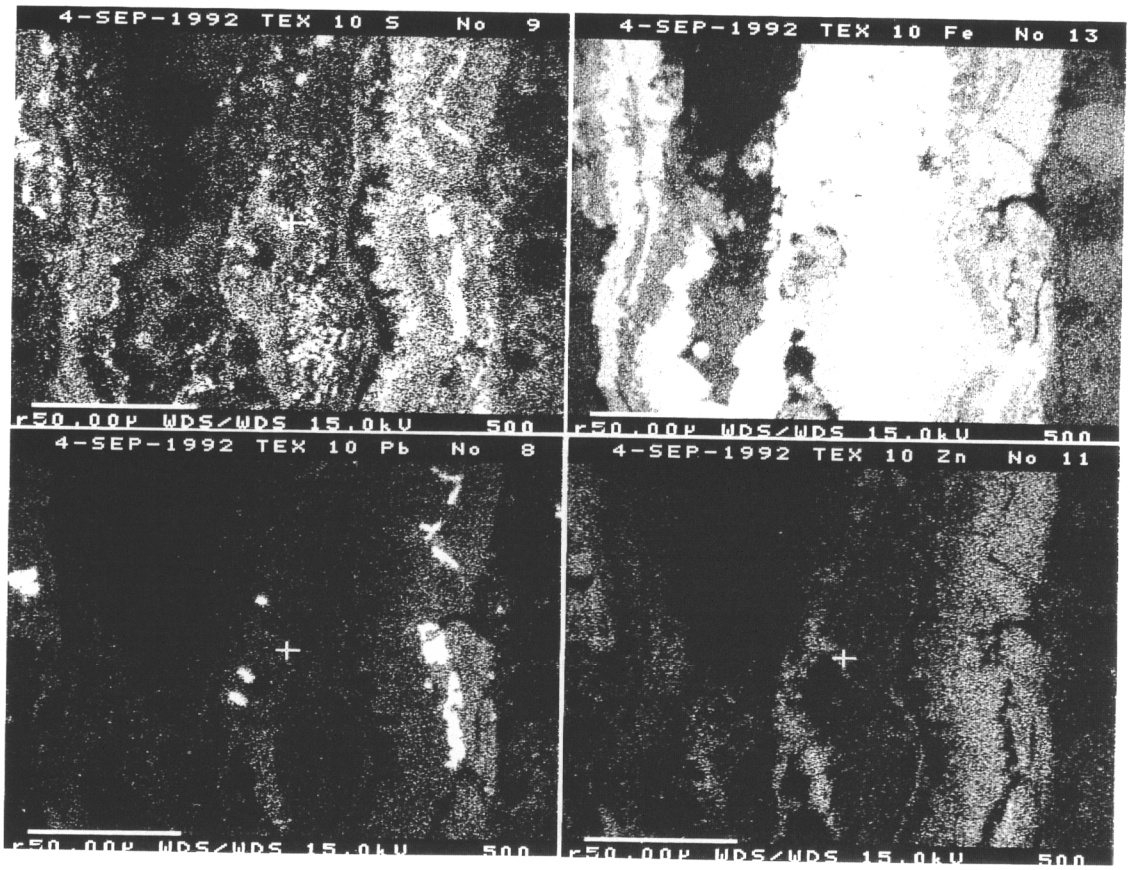

Figure 12. More x-ray maps of the clarifier bottoms in Sample #10.

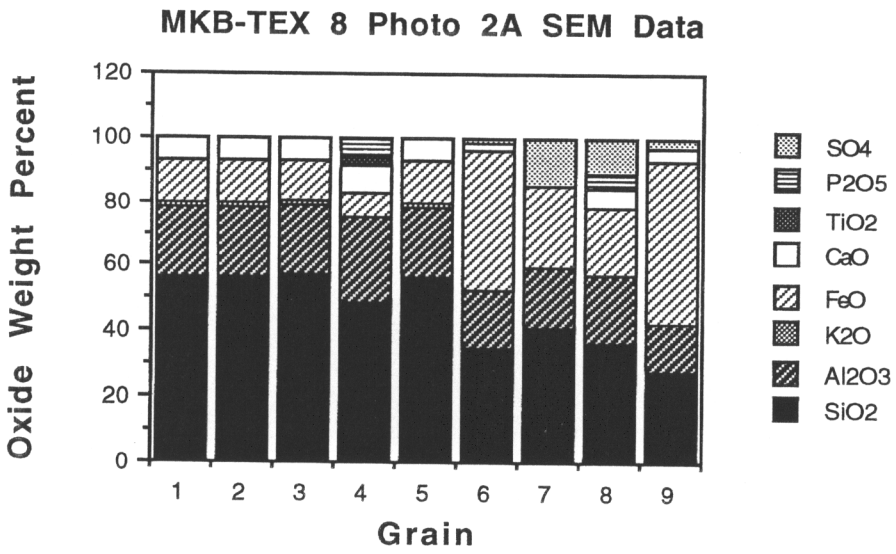

Figure 13. This bar graph is of SEM data for some grains analyzed in a region of Sample #9 (clarifier bottoms). Grain numbers at the bottom of the graph correspond to grains analyzed.

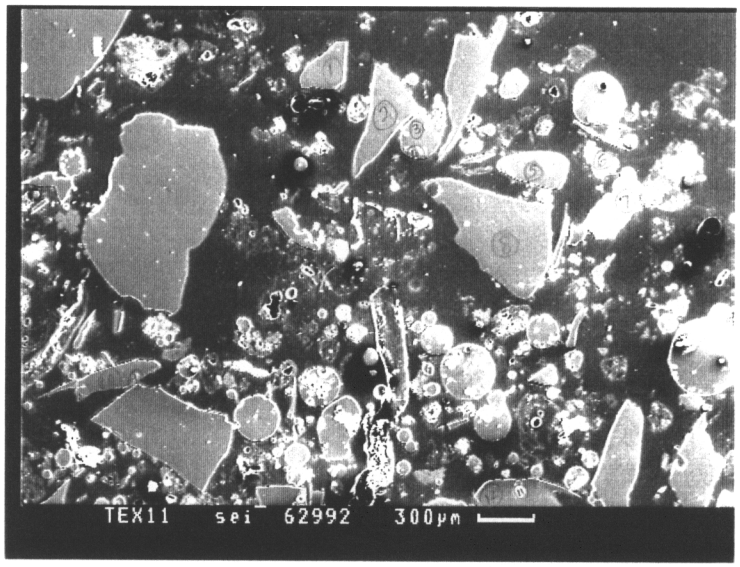

Figure 14. Typical nature of the material found in the lock hopper fines (Sample #11). Photo is a secondary electron image produced on the SEM.

samples in a matrix of Si-Al-Ca-Fe oxide glass (see Figure 5). A "fingerprint-like" texture occurs in the slurry before it is gasified , as can be seen in Sample #1 (see Figure 15), a dried sample of the raw material. Some samples will be discussed below along with appropriate figures in the order that the samples occur in the system.

Sample #1, which is the feedstock material, has bright areas on the backscattered electron image (Figure 16) illustrating the "droplet" nature of the pyrite within the glass. Figure 17 shows a segregation of FeS_2 and clay into two separate halves of a single grain. Weathered feldspar fragments in clays can be seen in Figure 18. The mineral assemblage in the coal can be seen in Figure 15 where the brightest areas are mostly composed of an iron oxide, the medium bright areas are possibly grunerite ($FeSiO_3$), and the dull background is a clay. These textures have little to do with those of the slag, as this material is the uncombusted slurry of PVSS and coal.

Figure 19 shows the porous nature of **Sample #2**. The solid masses in Figure 19A are Si-Al-Fe-Ca oxide glass. X-ray maps (Figure 20) produced on the electron microprobe illustrate the distribution of Fe, S, Zn, and Si in two regions of this sample. Note the tendency of the Zn to rim the larger grains rather than be contained within them.

As noted above, **Sample #3** contains skeletal crystals of both sphalerite and spinel (see Figures 2 and 3). These skeletal crystals are probably a result of exsolution of these phases from the glass. Rims of PbS can be found around some grains such as is illustrated in Figure 21 (same area as Figure 3).

Figure 22 shows x-ray maps of one of the cruciform spinels found in **Sample #4**. Note how the bulk of the Cr is confined to the core of the crystals, surrounded by a protective Al reaction rim.

The remainder of the samples had fewer mineral analogs in similar glass matrices, with no unique textures not already seen in the samples described above.

Reactions With Refractories:

Over time, some refractory materials react with the inorganics. This usually results in spalling of the outermost layer of the bricks. Some of the Cr may have come from this, while the remainder may arise from the original composition of the materials of the ash which varies somewhat over time.

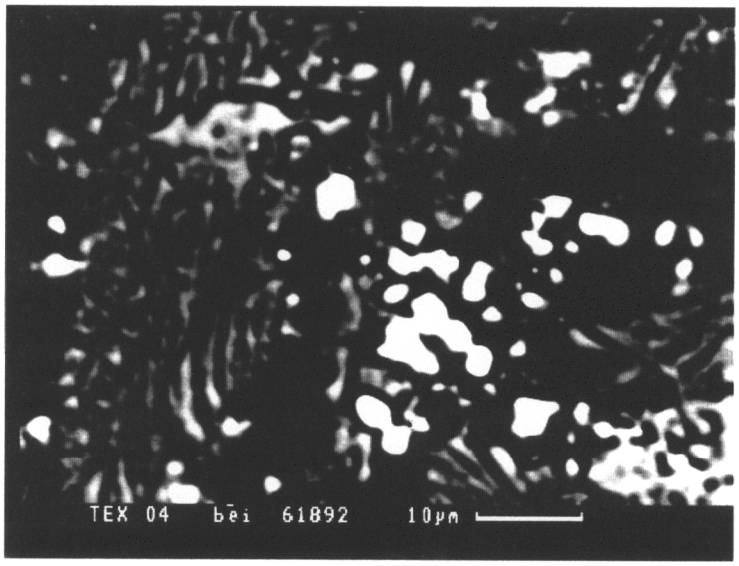

Figure 15. "Fingerprint-like" texture found in the slurry before it is gasified. Photo is a backscattered electron image produced on the SEM of Sample #1.

A.

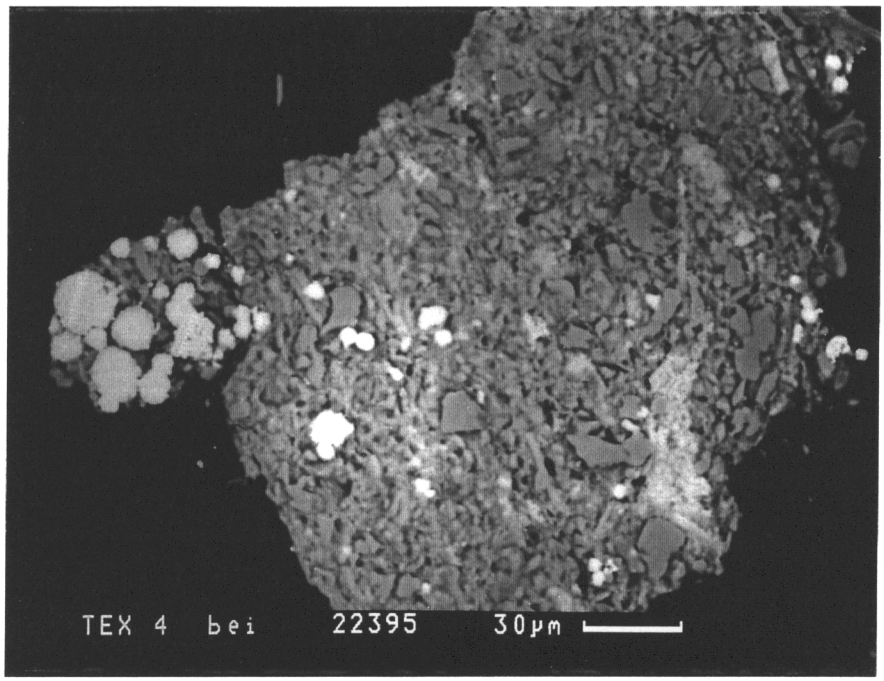

B.

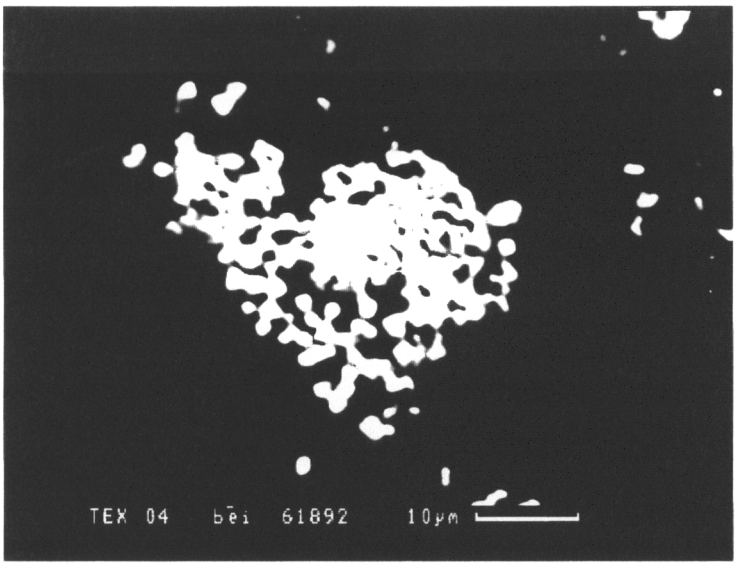

Figure 16. Backscattered electron images produced on the SEM of two areas of Sample #1 (the dried raw material) showing the "droplet" nature of pyrite (brightest areas). Photo B is a good example of pyrite replacing the original wood cells in the coal.

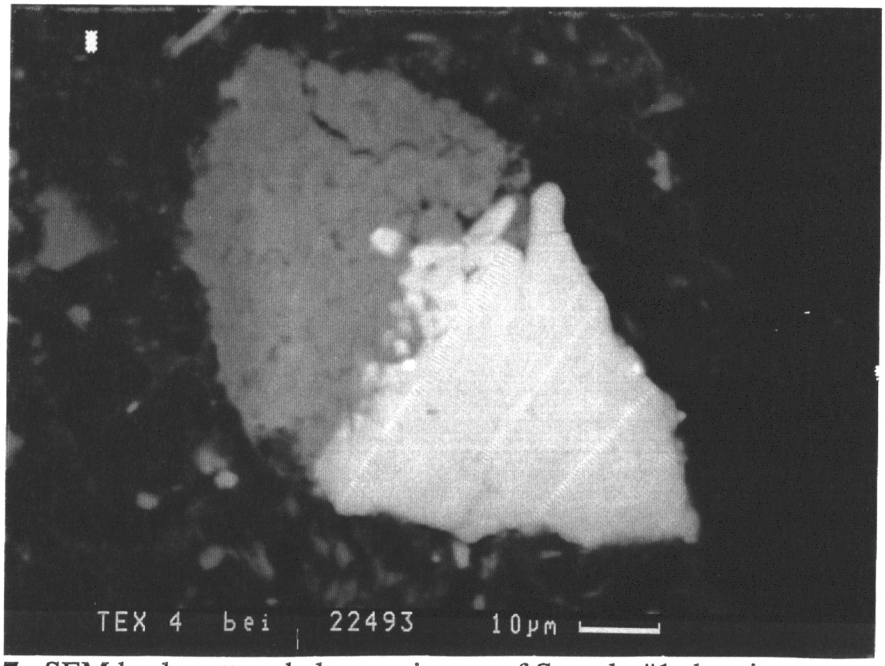

Figure 17. SEM backscattered electron image of Sample #1 showing segregation of pyrite (bright area) and clay (dull area) within a single grain.

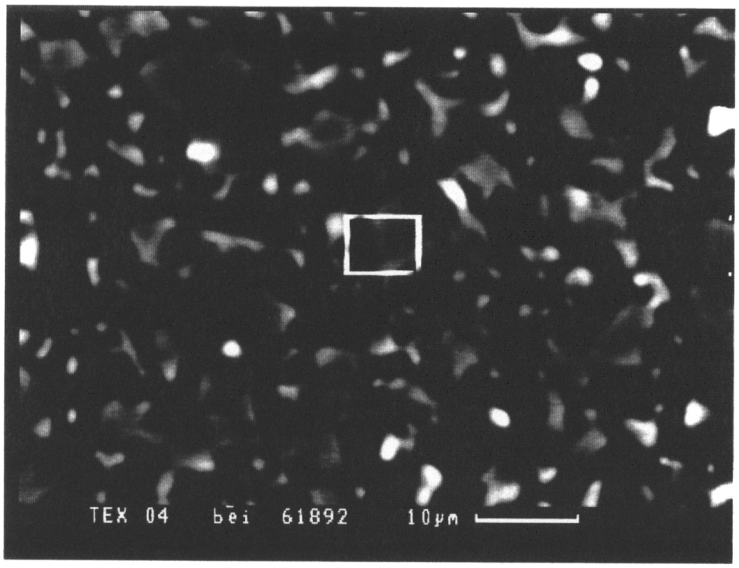

Figure 18. SEM backscattered electron image of Sample #1 showing the remnants of weathered feldspars surrounded by clays.

A.

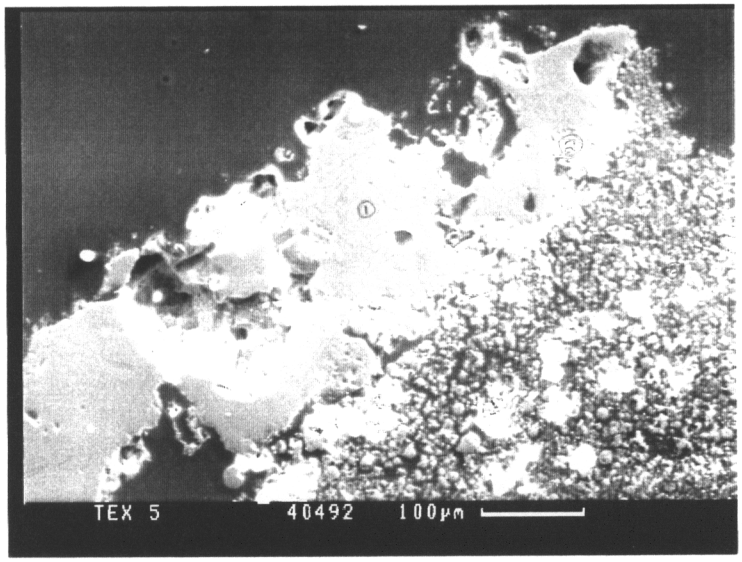

B.

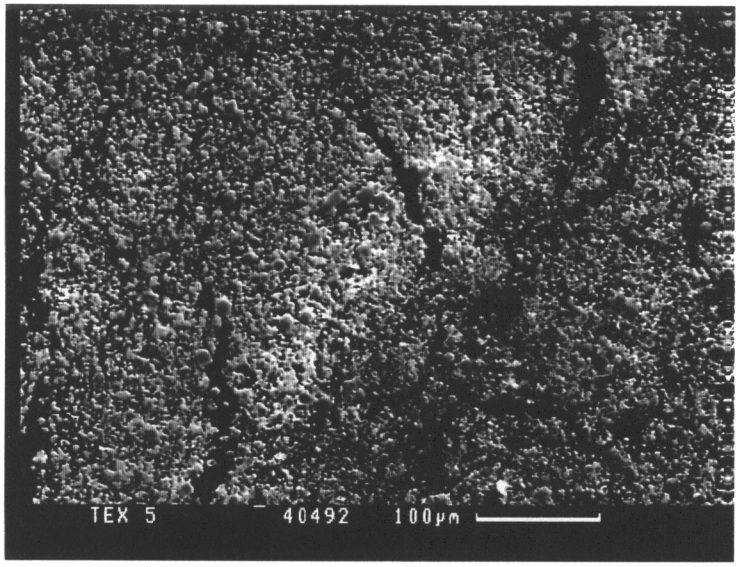

Figure 19. SEM secondary electron images of Sample #2 showing the porous nature of this material. Both Pb and Zn oxides were found in the area covered by Photo B.

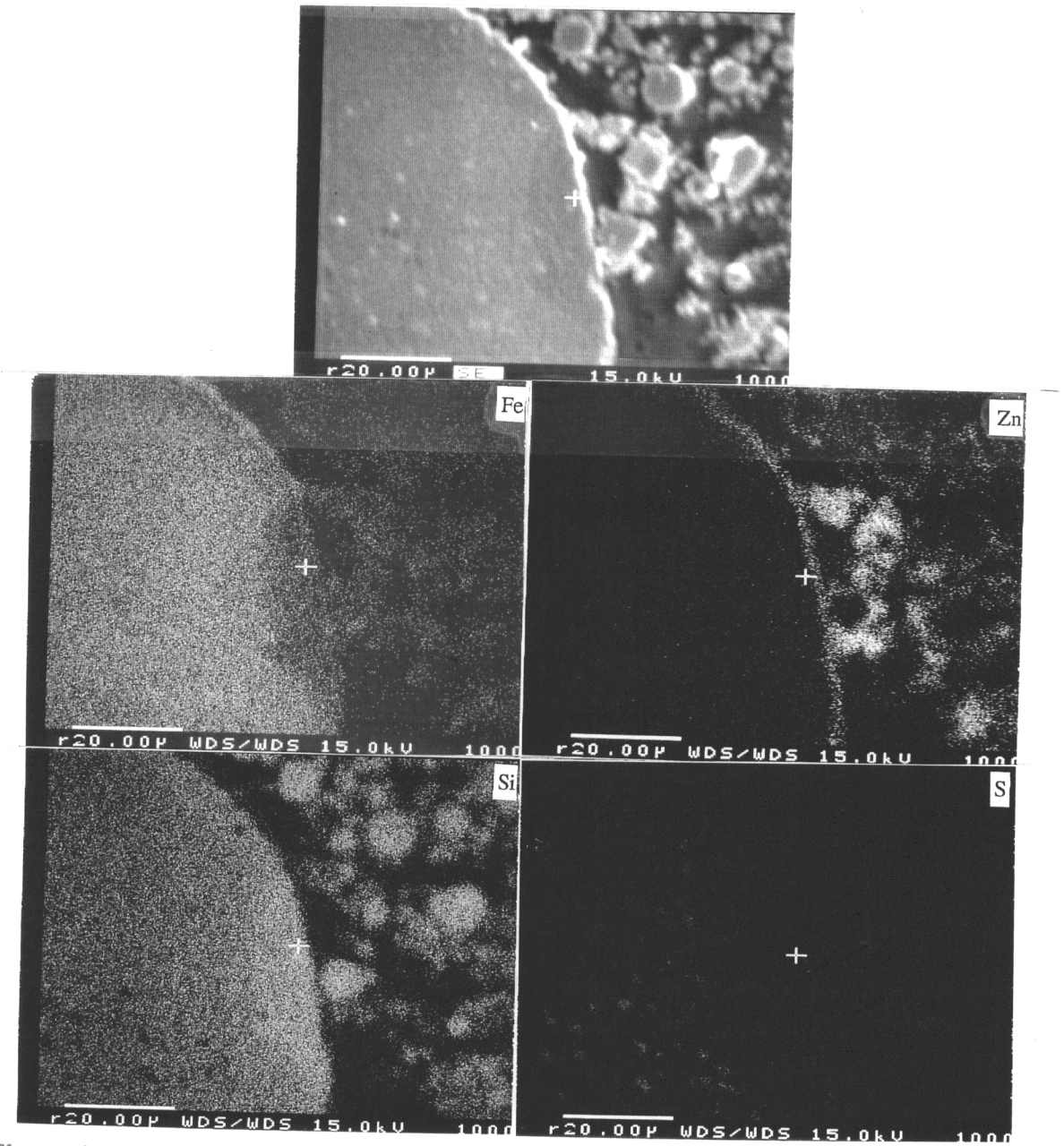

Figure 20. Area of Sample #2 examined with the microprobe. Top photo is a secondary electron image of a large grain surrounded by smaller grains to the right. Other photos are Fe, Zn, Si, and S x-ray maps of the same region. Note how the Zn tends to be concentrated in the rim of the large grain and within the small grains.

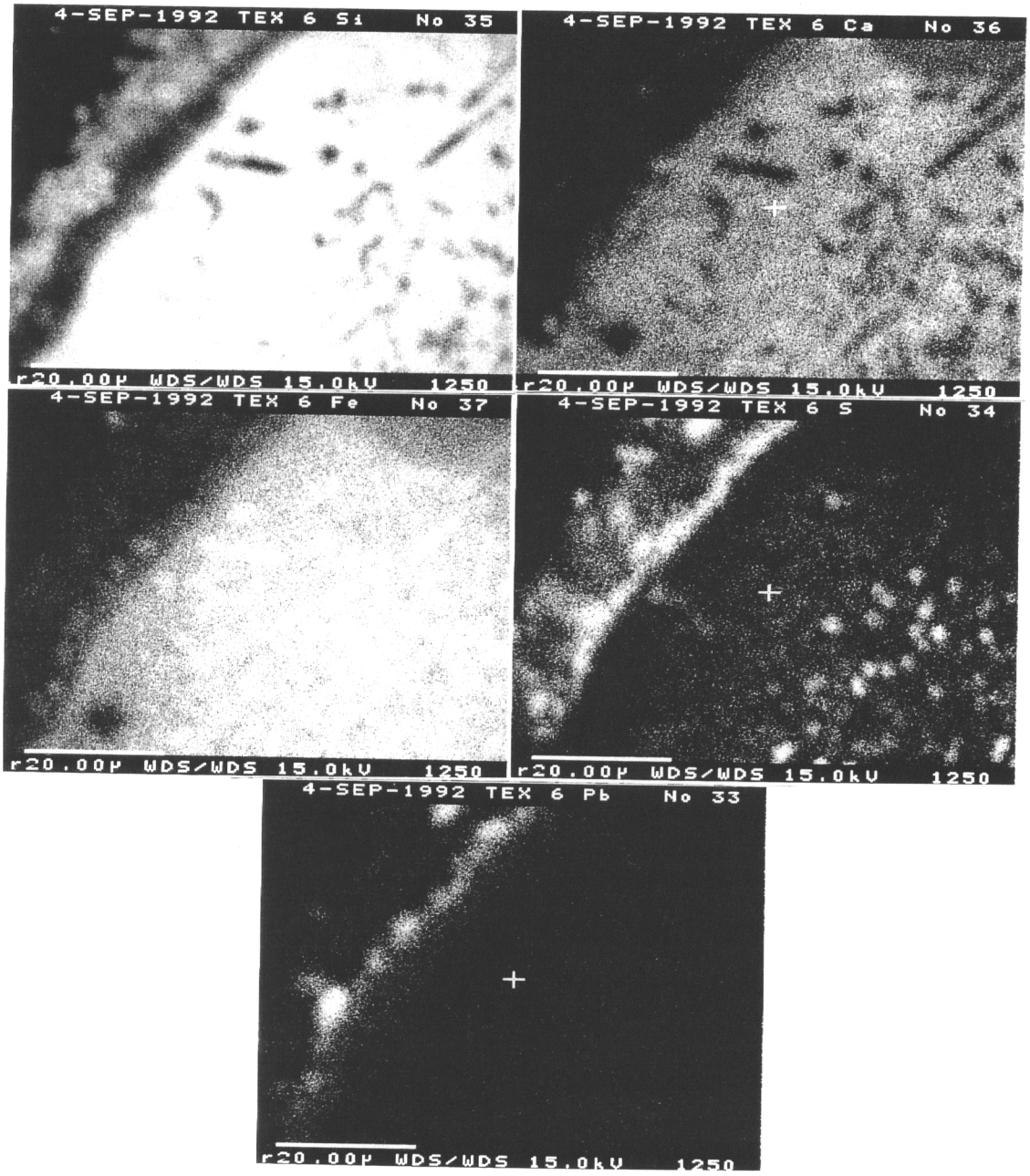

Figure 21. X-ray maps of Si, Ca, Fe, S, and Pb, produced on the microprobe, of a grain boundary in Sample #3. Note how Pb, probably as PbS, rims the grain. These maps are of the same region as those in Figure 4.

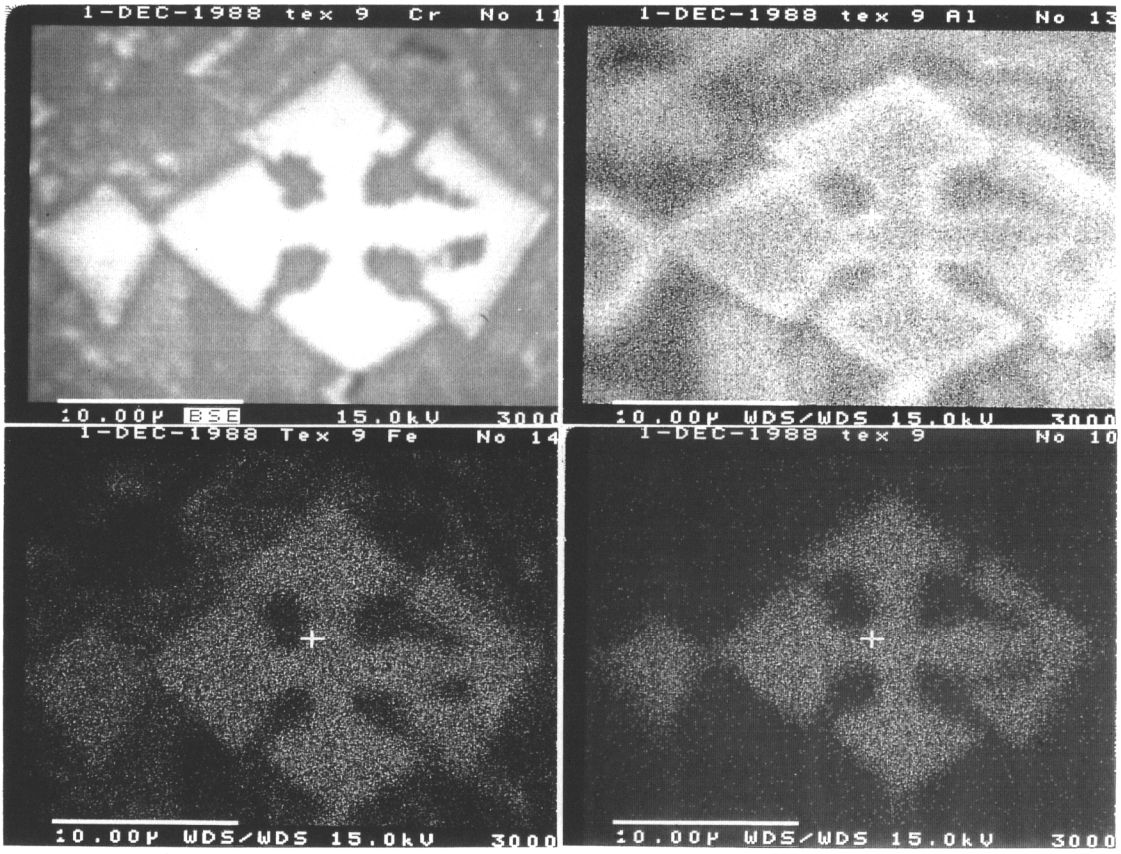

Figure 22. Top left photo is a backscattered electron image produced on the microprobe of a spinel in Sample #4 (throat deposit). The three other photos are x-ray maps of the major cations, Al, Fe, and Cr, in these spinels. Note the core of these cruciform crystals is Cr, surrounded by a protective coating of Al.

Discussion:

Mostly Si-Fe-Al-Ca oxides were found in the form of inert glasses with a few spinel type oxides present and minor amounts of sulfides. This was expected because this ash was the residual primarily of the inorganic fraction of coal concentrated 10 to 20 times. The majority of the ash was in a glass phase as the bulk composition was above the solidus and the ash cooled relatively rapidly as compared to normal geologic cooling rates.

There was a common presence of spinels with compositions ranging from Fe-Cr-Al to Fe-Al. These are typically the first phases formed on cooling of the glasses, somewhat analogous to volcanic rocks.

Pb and Zn occur as both oxides and sulfides. Insufficient amounts of S were retained to tie up all Zn as ZnS and Pb as PbS; therefore oxides formed also. Zn oxide and sulfide were both found in the clarifier bottoms in sample #8, suggesting that the system was near the border between these two phases on the phase diagram. ZnO was also found in the lock hopper fines (sample #11), but no S was found; this suggests that this part of the system is well within the oxidized region on the phase diagram.

Zoning of crystals was noted in several cases, suggesting changes in the equilibrium of the system on occasion. In sample #4, the cruciform spinels exhibited zoning with cores rich in Cr which were surrounded by outer rims rich in Al, suggesting that as the system became depleted in Cr more Al was incorporated into the spinel structure. Zoning of ZnS in the cooling coil sample (#3) of Zn and Fe was possible on a submicroscopic level as S levels changed in the presence of Fe and Zn, which could explain the amounts of Fe found in these tiny crystals using the SEM. Zn and Pb were found to rim large Si-rich oxide glass grains in samples #2 and #3 from the burner face and cooling coils, respectively.

A very small amount of the ash is expected to react with the surface layer of the refractory bricks during normal operation. Cr was observed in Sample #4 which may have been due to this or to the Cr in the sludge ash. The Cr was found in cruciform spinel-type mineral analogs which are refractory in nature and generally had a protective Al rim covering the Fe-Cr rich core.

Municipal Solid Waste Ash Studies

Mode of Generation:

The second part of this study examined the characteristics of the ashes produced in three relatively typical municipal solid waste (MSW) incineration facilities as shown schematically in Figure 10. One group of samples was produced at an incineration plant which burns all MSW without any organized pre-burn separation beyond a voluntary community recycling program. Handling about 90,000 kg (100 tons) of mostly residential MSW per day, this plant mass burns the refuse in two furnaces that operate at approximately 1000°C (1832°F) to produce electricity and steam for space heating. Fly ash is collected and mixed with bottom ash on site and watered down to control dust. Kirby and Rimstidt (1993) have reported on leaching experiments of ash from this same facility.

A second group of samples was produced at an incineration plant which separates much of the aluminum, tin, plastics, glass, and large objects from the MSW prior to incineration for recycling and because their presence extracts otherwise useable heat from the system. This system has a burner operating in a negative atmosphere, producing approximately 650°C (1200°F) black smoke which is then sent to a chamber with additional air to combust the smoke. An auxiliary gas burner keeps temperatures above 980°C (1800°F) in the main chamber. The after burner stays about 1065°C (1950°F). Fly ash at this facility is also mixed with the bottom ash on site and dust is controlled by adding water.

A third group of samples was produced at an incineration plant which operates in much the same way as the first facility described above. No emphasis is placed on pre-sorting the MSW prior to incineration. The resulting ashes are handled in a similar fashion as at the other two facilities.

Bulk Chemistry and Concentration Factors:

Campbell (1990, a) projected that the United States would generate 190 million tons of MSW annually by the year 2000. However, an EPA report in July 1992, revealed that the United States actually surpassed this amount - reaching 195 million tons - in the year 1990, ten years before the generation of waste was supposed to reach this level (EPA, 1992). Only 16.3% (31.9 million tons) of this MSW was incinerated in 1990 (EPA, 1992). Of the remaining 83.7%, 66.6% (130.4 million tons) went to a landfill and 17.1%

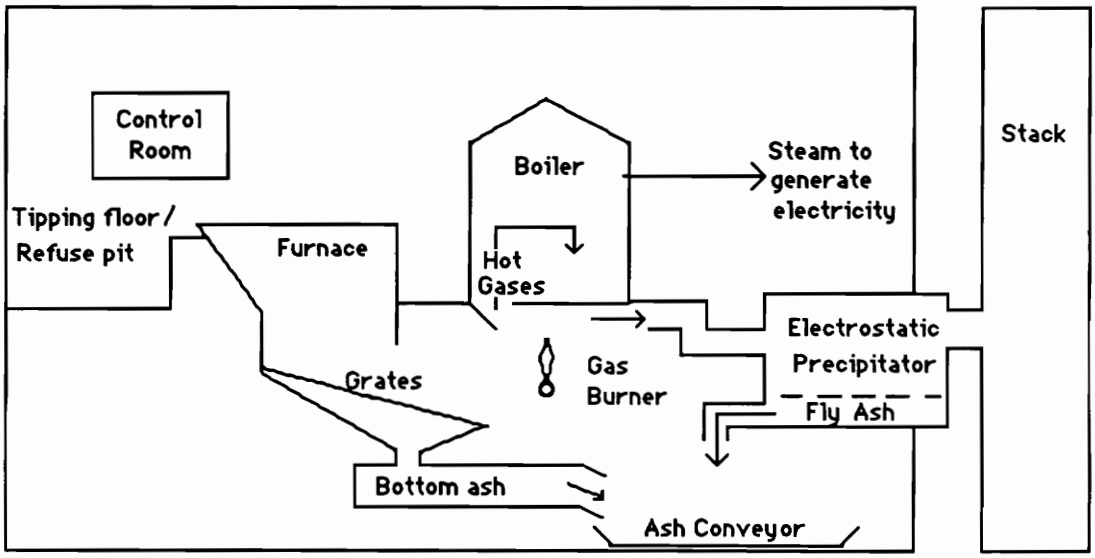

Figure 23. Schematic diagram of the basic layout of a MSW incineration plant.

(33.4 million tons) was recycled or composted.When MSW is incinerated, its volume is reduced by 85-90%, with a corresponding weight reduction of 65-80% (Bawkon, 1991). Figure 24 is a schematic diagram illustrating some background information on the major subdivisions of MSW and how they react during incineration.

Bulk chemical analyses of MSW ashes reveal that samples are composed predominantly of Si, Fe, Na, Ca, and Al oxides which compose approximately 50-60% of the ash in the form of glasses. Minor concentrations of Pb, Sn, and Cr can be found in some samples and tend to concentrate in crystalline phases rather than in glasses. Table 3 presents the detailed bulk chemistry of ash from the first incinerator described which does no separations prior to burning (from Kirby and Rimstidt, 1993).

Phases and Mineral Analogs:

Approximately 50-60% of the MSW ash consists of a Si-Fe-Na-Al-Ca glass (see Table 1, Appendix B for actual SEM data of glass compositions). The remainder of the material is composed of interspersed metals and mineral analogs, many of which exsolved or crystallized from a glass phase. Despite the enormous variety of phases present in MSW, the phases and mineral analogs present in the incinerator ash tend to be fairly consistent from one sample to another.

The most common crystalline phase and mineral analog found is cruciform skeletal spinel-type crystals which contain Fe as the major cation and variable amounts of the elements Cr, Al, Ti, Na, Si, and Mn as minor elements (see Table 2, Appendix B for SEM weight percent data). Their compositions range from 30.90 to 99.44 weight percent FeO, 0 to 63.94 weight percent TiO_2, always with less than 10 weight percent of each of the remaining elements. Figure 25 shows the wide range of forms exhibited by these phases as they exsolved from a glass phase. Another very commonly observed mineral analog is olivine (Fe_2SiO_4) which occurs as broken blades with a poikilitic texture making them appear to be elaborate ladders (see Figures 25 and 26). Macroscopic pieces of Si-Al-Fe ceramic which apparently possess melting points above incineration temperatures have survived into the ash intact. Occasionally, there was encountered an alloy bearing Si, Ti, Pb, and Sn which probably came from soldered joints in tin cans. Euhedral crystals, in several forms, of olivine ($CaFeSiO_4$) are also present in the glass (see Figures 25 and 27). The only sulfide minerals commonly encountered are pyrite and pyrrhotite which are found as inclusions in glass (see Figures 28 and 29).

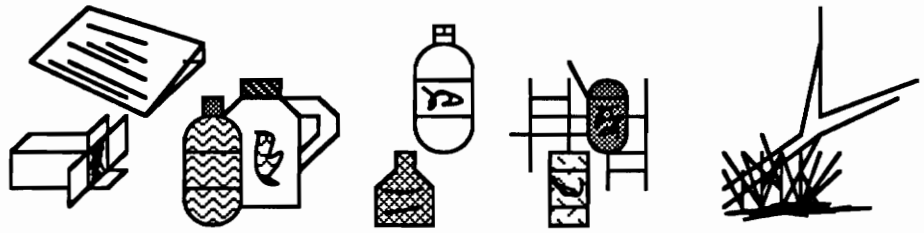

	Paper	Plastics	Glass	Metals	Yard Waste
Average weight%*	37.5	8.3	6.7	8.3	17.9
Average volume%*	32	21	2	11	10
Typical elements and compounds contained	Clays, C, Ca, SiO_2, Al, TiO_2	Clays, Micas	SiO_2, Na_2O, Borate	Al, Fe, Sn, Cu, Pb, Mg, Hg, Cr, Cd, Zn, Ni, Mn, ...	C, SiO_2, Al_2O_3, H_2O
Reduction during combustion	95-99%	95-99%	0%	0%	80-95%
Concentration factor during combustion	20-100x	20-100x	0x	0x	5-20x
Losses during combustion	CO_2, H_2O	CO_2, H_2O, HCl, Na	Na	Hg, Zn, Cd, Pb	CO_2, H_2O
Residuals after combustion	TiO_2, SiO_2, Al_2O_3, CaO	FeO, SiO_2, Al_2O_3, CaO	SiO_2, B	Al_2O_3, FeO, SnO, CuO, CrO	FeO, SiO_2, Al_2O_3, Cl, Na_2O

Figure 24. Schematic outline of MSW combustion.
* Neither volume nor weight percents add up to 100% because of an "other" category not listed here.

Table 3. Bulk chemical analysis of ash and the corresponding estimated weight percent of oxides in the glass fraction from Kirby and Rimstidt (1993). LOI is loss on ignition.

Species	Weight Percent	Estimated Wt% in Average Glass
SiO_2	33.4±0.8	49
Al_2O_3	13.4±6.6	13
LOI	9.7±4.6	10
CaO	9.1±1.0	11
Fe_2O_3	8.7±3.6	4
Na_2O	4.2±0.2	5
SO_4	3.5±0.8	1
K_2O	1.7±0.4	2
TiO_2	1.6±0.1	0.02
MgO	1.5±0.4	1
ZnO	>1.25±?	1
P_2O_5	1.1±0.52	1
Cl	1.04±0.08	1
PbO	0.41±0.12	0.4
MnO_2	0.24±0.08	0.2
Cu_2O	0.22±0.06	0.2
BaO	0.12±0.06	0.1
B_2O_3	$5.5\pm0.4\times10^{-2}$	1×10^{-1}
Cr_2O_3	$5.0\pm0.4\times10^{-2}$	1×10^{-1}
SrO	$2.6\pm0.2\times10^{-2}$	2×10^{-2}
CdO	$1.6\pm0.6\times10^{-2}$	1×10^{-2}
SnO_2	$1.4\pm0.2\times10^{-2}$	1×10^{-2}
NiO	$1.4\pm0.6\times10^{-2}$	1×10^{-2}
V_2O_5	$1.1\pm0.4\times10^{-2}$	1×10^{-2}
Ag_2O	$3.0\pm1.8\times10^{-3}$	2×10^{-3}
CoO	$2.3\pm1.2\times10^{-3}$	2×10^{-3}
SeO_2	2.0×10^{-3}	1×10^{-3}
Hg	5.0×10^{-4}	3×10^{-4}
Au	5.0×10^{-5}	3×10^{-5}
Total	91.3±9.0	

A.

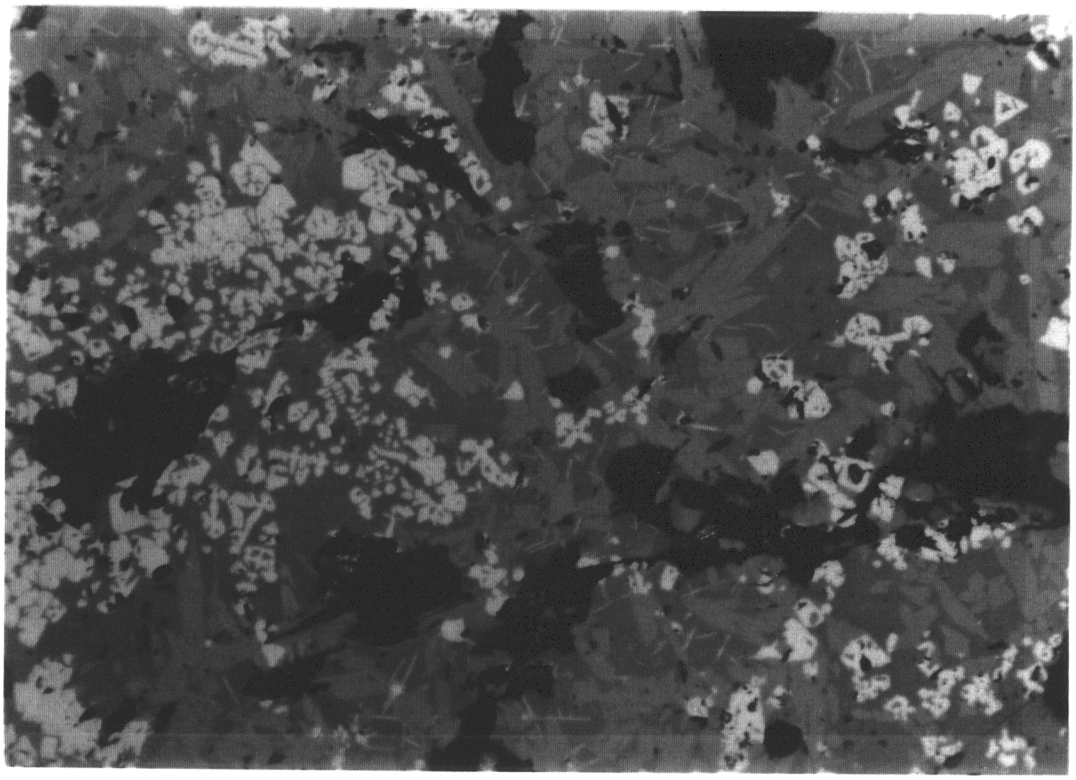

B.

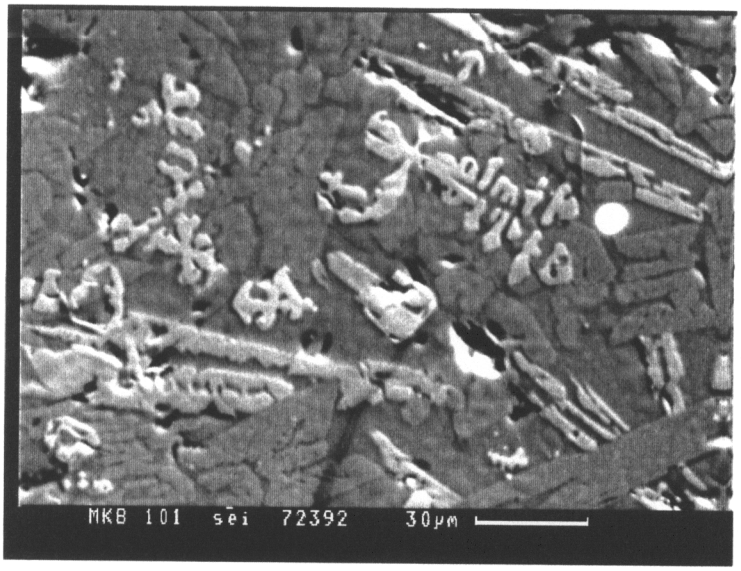

Figure 25. Skeletal spinel crystals show a variety of forms in the MSW ash. Photo A was taken on the light microscope. Photos B and C are SEM secondary electron images. Photos D-H are SEM backscattered electron images. Also seen in these photos are euhedral and "ladder" forms of olivines.

C.

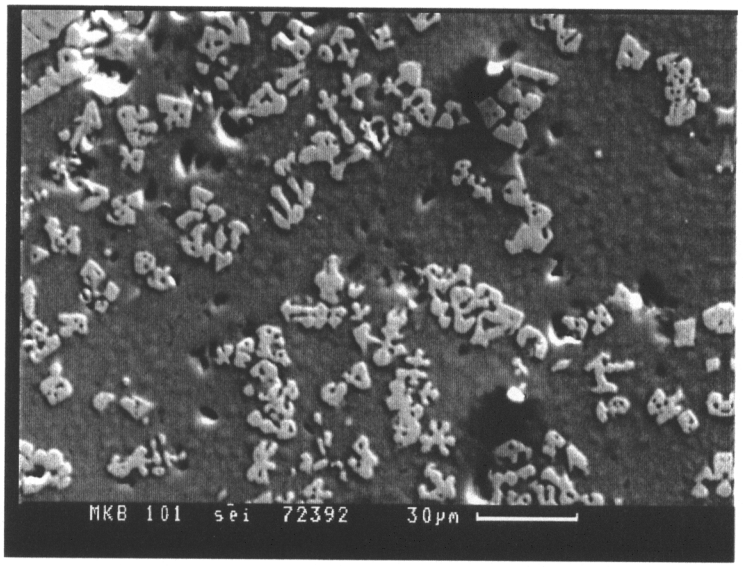

D.

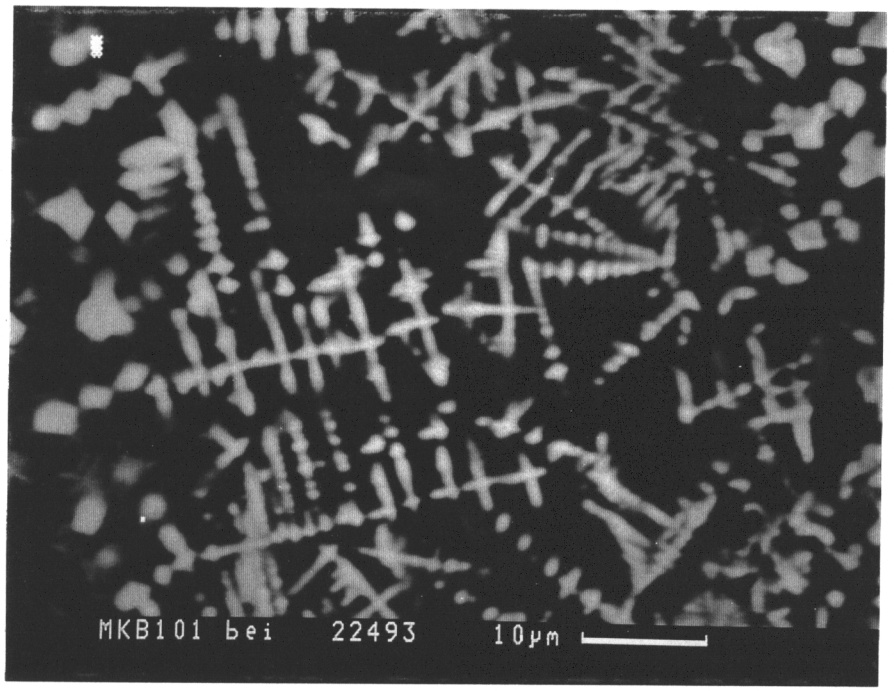

Figure 25. Continued from previous page.

E.

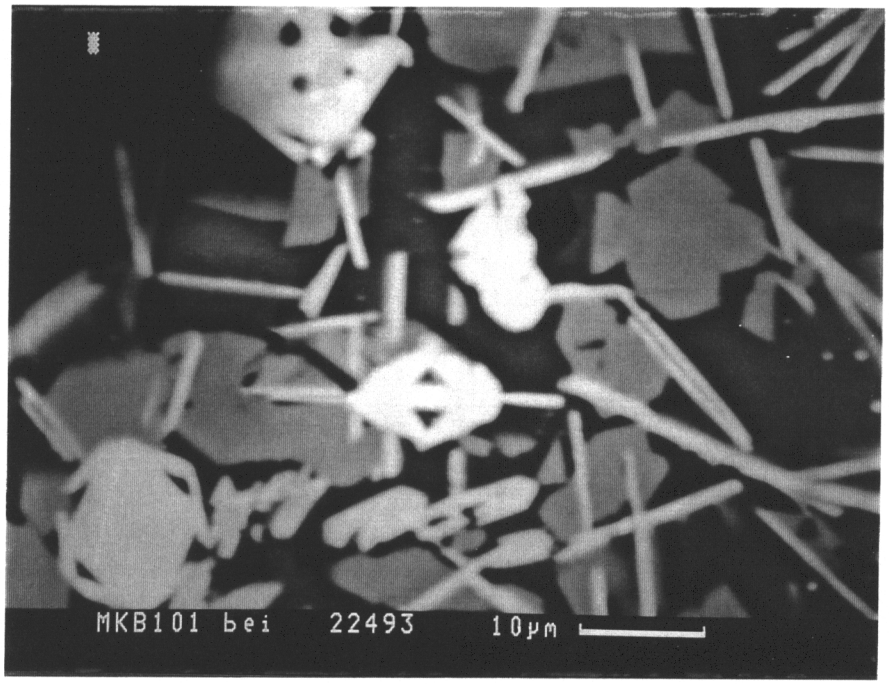

F.

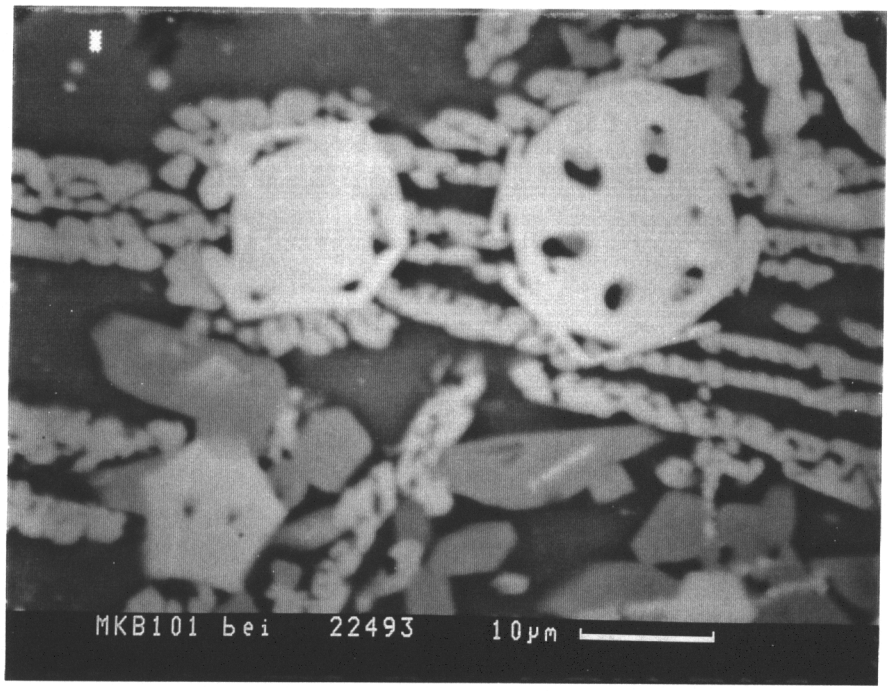

Figure 25. Continued from previous page.

G.

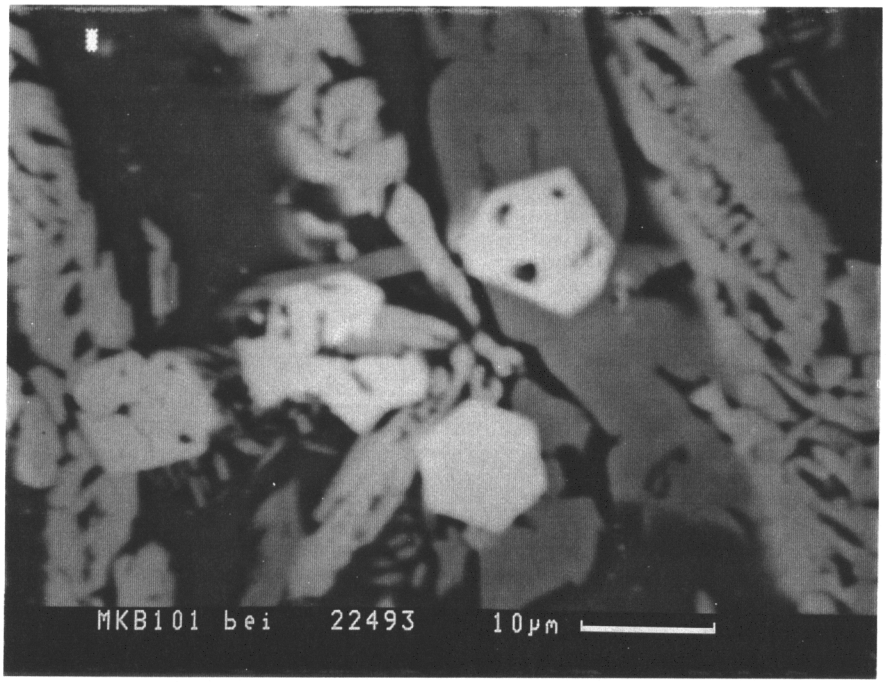

H.

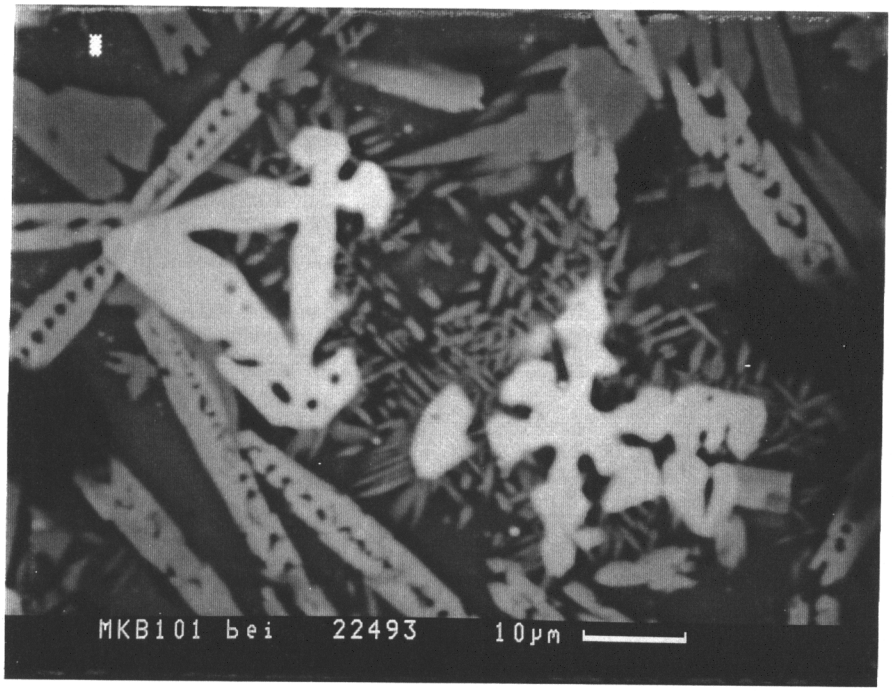

Figure 25. Continued from previous page.

A.

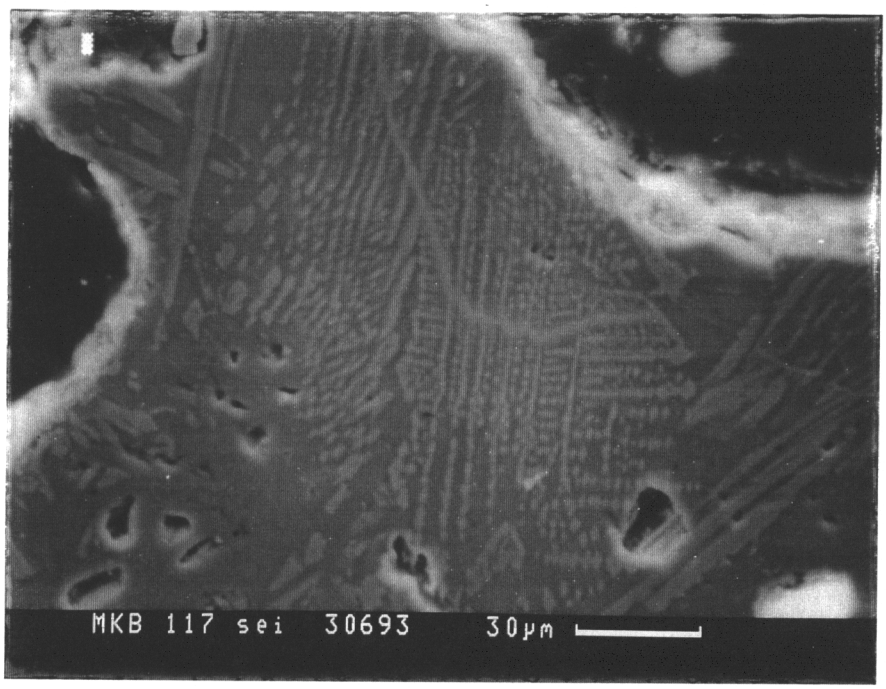

B.

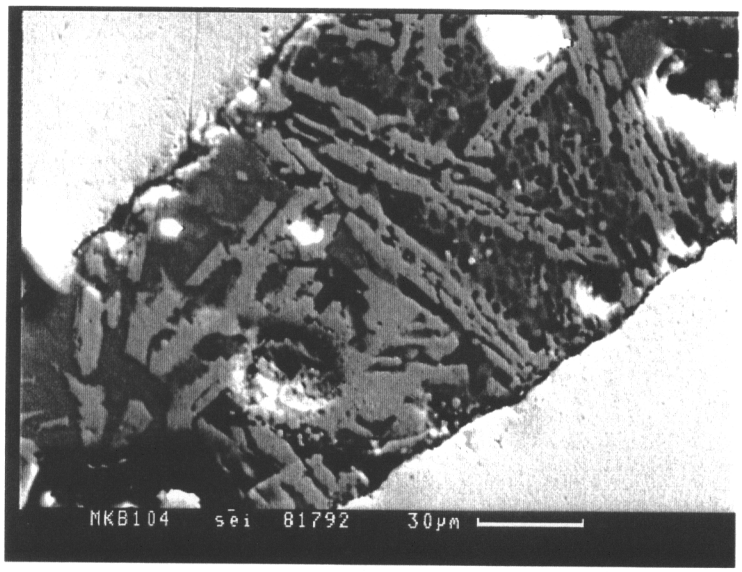

Figure 26. Olivine (Fe_2SiO_4) blades and "ladders" exsolved from the glass. Photos A and B are SEM secondary electron images.

A.

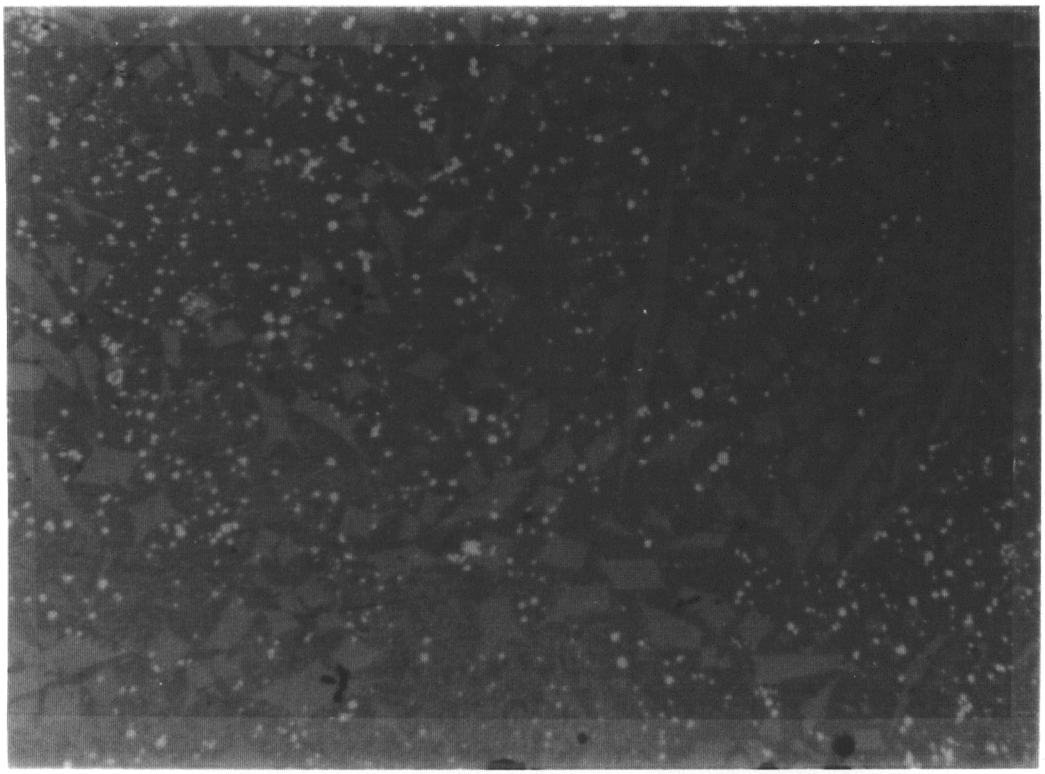

B.

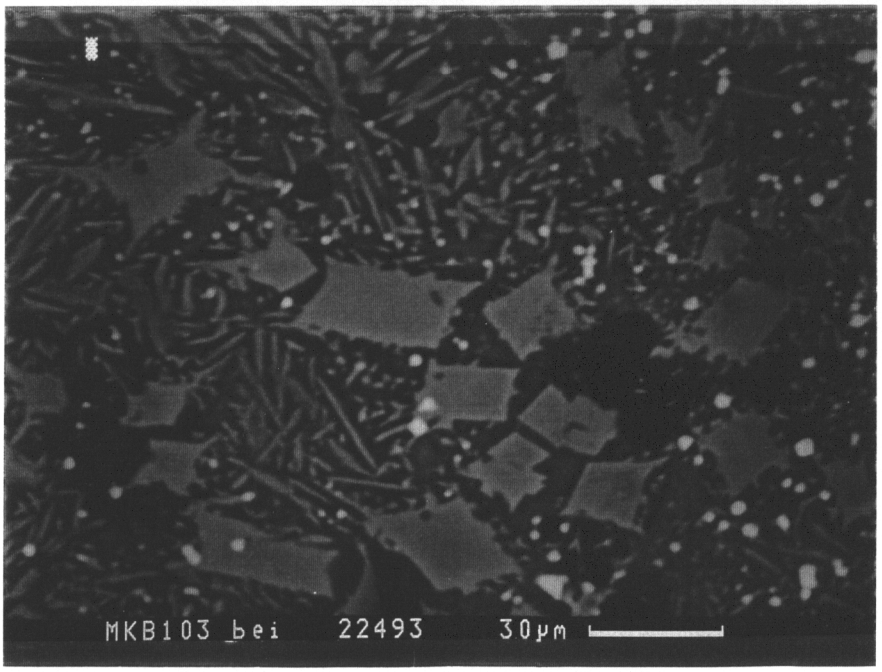

Figure 27. Euhedral to subhedral olivine ($CaFeSiO_4$) crystals which formed early in the solidification of the ash. Photo A is a light microscope image. Photo B is a SEM backscattered electron image.

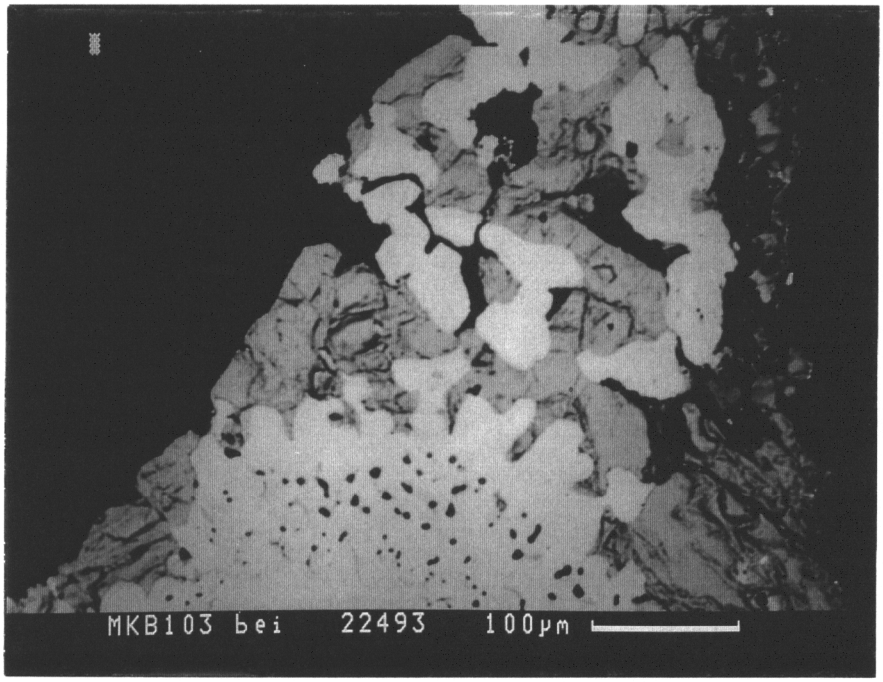

Figure 28. SEM backscattered electron image illustrating the typical nature of pyrite (FeS_2) found in the MSW ash.

A.

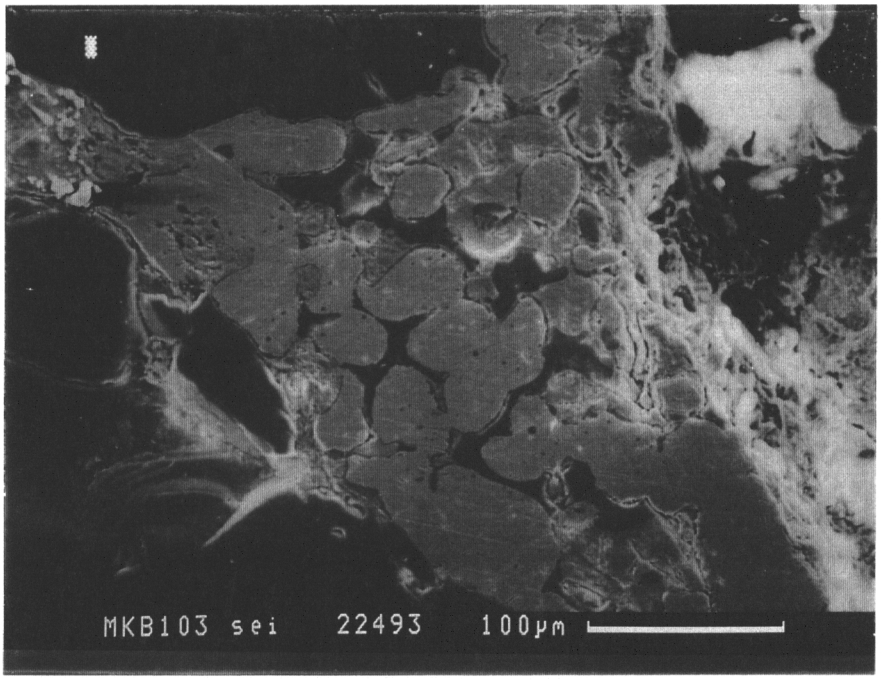

B.

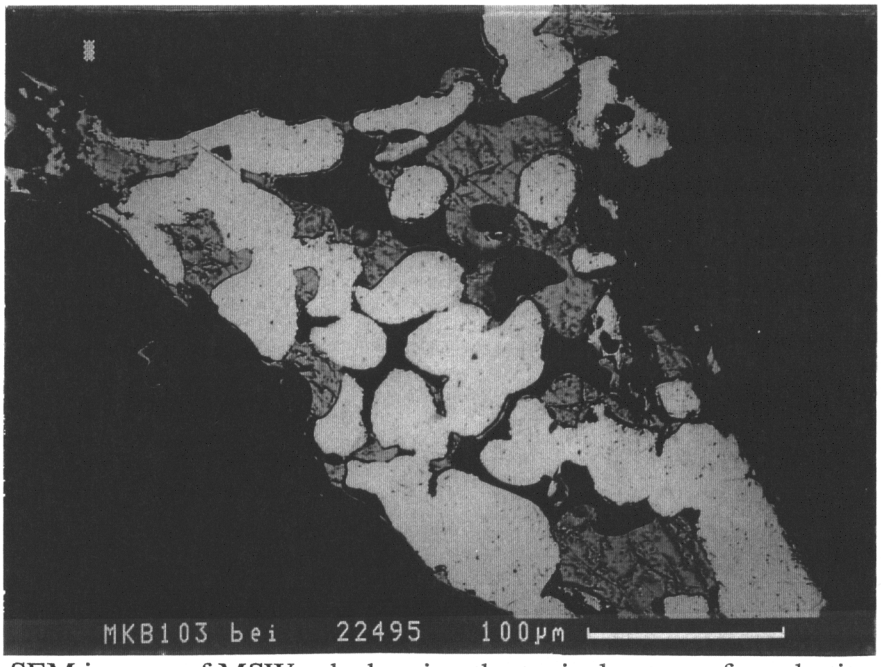

Figure 29. SEM images of MSW ash showing the typical nature of pyrrhotite and native iron. Photo A is a secondary electron image. Photo B is a backscattered electron image of the same area. Brightest spots on photo B are of the native iron.

In most of these samples at least one of several metals can be found. Subhedral to anhedral crystals of silicon carbide can be found within a matrix of suspected aluminum carbide (see Figure 30). This aluminum phase can be observed, using a reflected light microscope, effervescing when water is placed on it. The original Al-Si area is white to tan but the Al area quickly becomes a mix of green, blue and violet when water is placed on the surface of the sample. Microprobe investigations of these Al-Si patches revealed only Al and Si, respectively, and hence were inconclusive as to the identity of this material because the element suspected, carbon, is not detectable on the microprobe. Native Fe was present in some samples (see Figure 29), usually in an assemblage with an Fe sulfide (FeS).

Samples from the three facilities contained fairly consistent phase assemblages, with few variations from one facility to another. Most all samples contained trace amounts of Ti in just about all phases. In one sample from the third facility, a grain 120 x 30 microns in size was found which was 97 weight percent Au, 3 weight percent Al (see Figure 31). No patches of the reactive Al-Si material were found in the ash from the facility which presorts, although it was found in the material from the other two plants.

Kirby and Rimstidt (1993) have confirmed the presence of several mineral analogs using separates and concentration techniques to purify the material enough for XRD to be effective. Table 4 summarizes their results and compares those results to the ones of this study.

Textures:

Most of the textures found seem to indicate that the bulk of the mineral analogs have exsolved from a glass. The photos in Figure 25 are representative of the many skeletal cruciform patterns formed in the glass as the spinels have exsolved. No consistent pattern could be discerned linking minor trace element compositions in the spinels to certain skeletal shapes. The open, ladder-like crystals of olivine as seen in Figure 26 are also probably the result of exsolution. Euhedral crystals of olivine take several shapes as seen in Figure 27, probably crystallizing while temperatures were still above that of the stability field of the other phases in this system. A subhedral, non-skeletal magnetite grain, with no trace elements present, and another magnetite with 10 weight percent Ti were found that appeared to have been corroded away on all sides, illustrating that they were not in equilibrium with the surrounding glass (see Figure 32).

A.

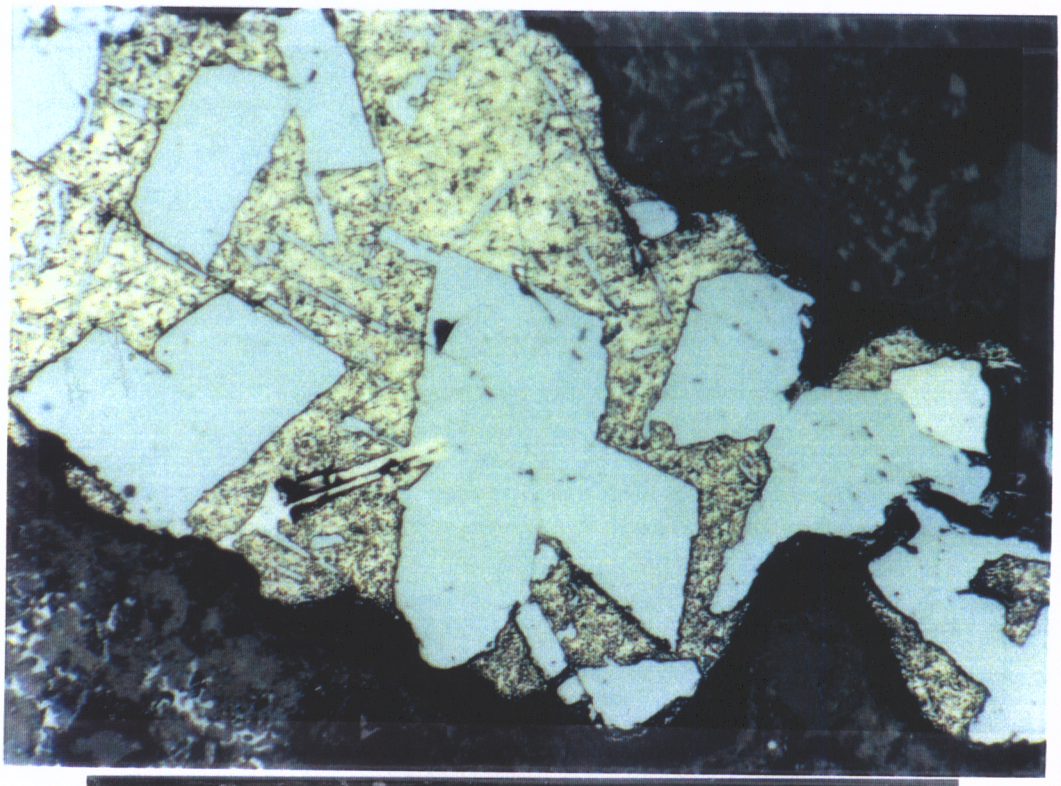

B.

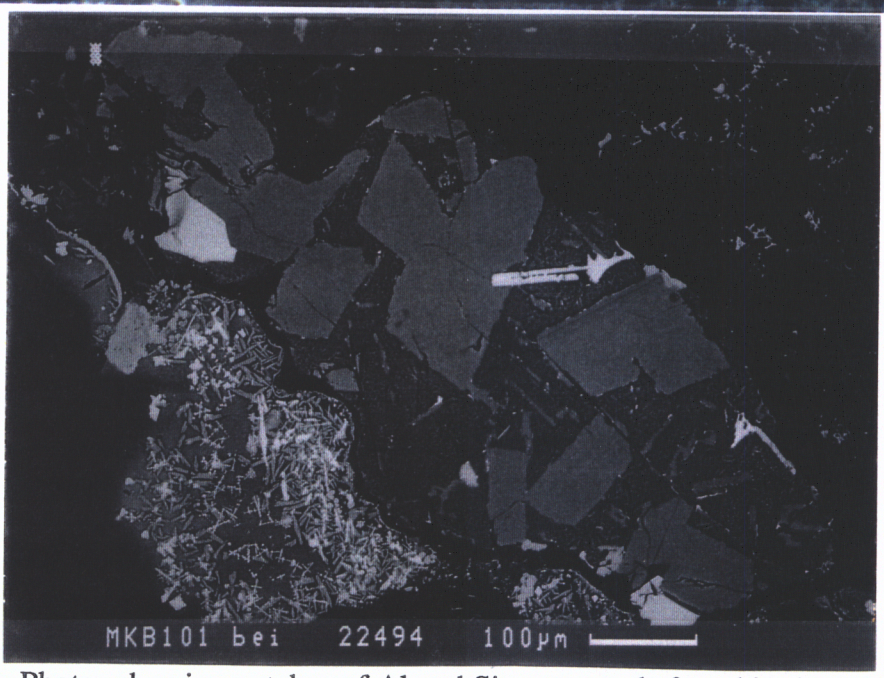

Figure 30. Photos showing patches of Al and Si compounds found in the ash from two of the facilities. Al groundmass is highly reactive in water. Photo A is a light microscope image. Photo B is a SEM backscattered electron image of the same area.

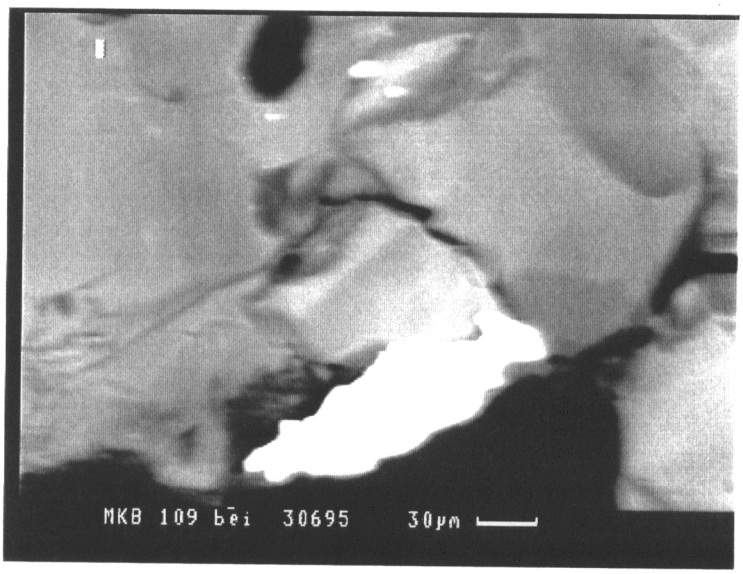

Figure 31. SEM backscattered electron image of a 97 weight percent Au, 3 weight percent Al grain found in the MSW ash.

Table 4. Phases and mineral analogs found in this study and those found by Kirby and Rimstidt (1993). "X" indicates the phase was observed, "--" indicates the phases was not observed, "possible" indicates the necessary elements were present in SEM analyses but were never observed alone instead mixed with a glass phase.

Phase	Mineral Analog	This Study	Kirby and Rimstidt
Fe_2O_3	Hematite	X	X
$CaCO_3$	Calcite	--	X
NaCl	Halite	possible	X
SiO_2	Quartz	X	X
AB_2O_4	Spinel - magnetite	X	X
TiO_2	Rutile	X	X
$CaSO_4.2H_2O$	Gypsum	possible	X
$CaSO_4$.	Anhydrite	possible	X
$3(Al_2O_3).2(SiO_2)$	Mullite	possible	X
FeO	Wustite	X	X
KCl	Sylvite	--	X
$(Fe,Ca)_2SiO_4$	Olivine	X	--
$Fe_{1-x}S$	Pyrrhotite	X	--
FeS_2	Pyrite	X	--
Au	Gold	X	--
Al	Aluminum	X	--
$FeTiO_3$	Ilmenite	X	--
Fe	Iron	X	--
SiC	Silicon carbide	possible	--
AlC	Aluminum carbide	possible	--

A.

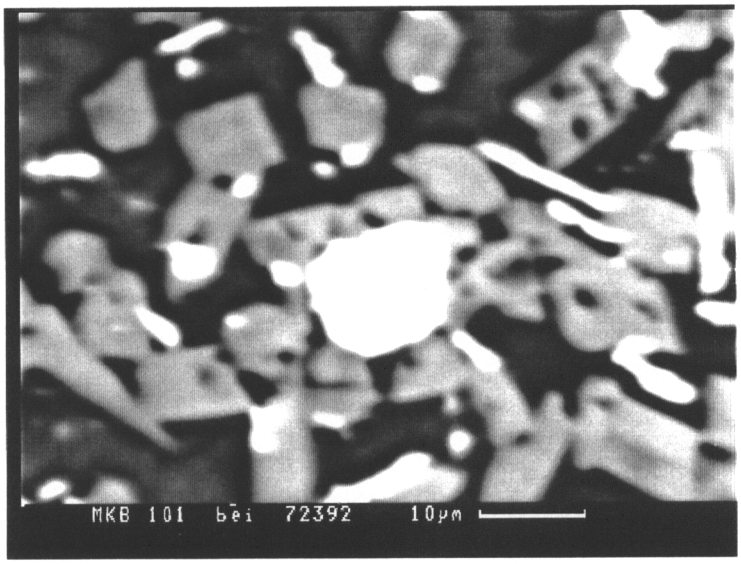

B.

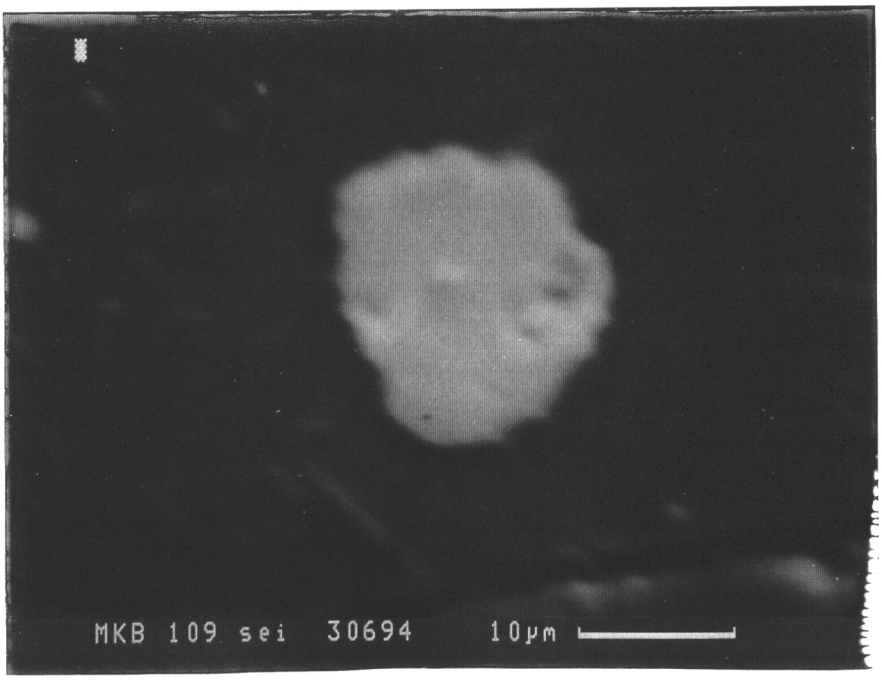

Figure 32. Photo A is a SEM backscattered electron image showing an corroded magnetite crystal surrounded by Fe, Ca-bearing olivine crystals. Photo B is a SEM backscattered electron image showing an "eaten" magnetite (10 wt% Ti) crystal surrounded by a Si-Ca-Al-Na glass. Both photos illustrate the disequilibrium in these two regions.

Reactions with Refractories:

Material growing on the surface of the refractory brick was sampled at the facility that presorts prior to incineration. Table 5 shows the bulk analysis of this material done over the area covered by Figure 33 on the SEM. A glass composed of Si, Al, and Ca oxides was found, containing grains of ilmenite (Fe-Ti-Mn-Mg oxide) and a Ti-Ca-Si spinel (see Table 3, Appendix B for SEM data). The slag collecting on the brick seems to be acting as a Ti sink, forming the Ti-bearing mineral analogs. The surface of the refractory brick still attached to the slag was very brittle and porous. This facility has had problems in the past with the deterioration of their refractory brick.

Discussion:

Despite the vast variety of phases burned, MSW ash samples were found to be relatively simple in terms of phases and quite similar regardless of source. The dominant phases were a glass commonly composed of Si-Al-Fe-Ca oxides, crystalline spinel phases rich in Fe and Ti, including magnetite, and Fe-Ca olivines.

Native metals, usually Fe as expected, were found. The native Fe was often found as very fine intergrowths with Fe sulfides, suggesting the system at that point was near the eutectic of these two phases. Native Au was also found, with approximately 3 weight percent Al which could be residue from the polishing process. Other metals found included Al and a Sn alloy. No visible Zn, Pb, or Cd phases were found.

The sulfides found were FeS_2 and $Fe_{1-x}S$. These were encased in glass and hence survived without oxidation.

Ti concentrations were nearly ubiquitous throughout all of the samples and probably came from paper products.

Table 5. Bulk analysis done on the SEM over the area covered by Figure 33 of the material growing on the refractory brick at one facility.

Compound	Weight %
SiO_2	40.66
CaO	18.81
Al_2O_3	23.51
FeO	4.84
TiO_2	4.89
MgO	4.00
P_2O_5	2.88
Na_2O	0.43

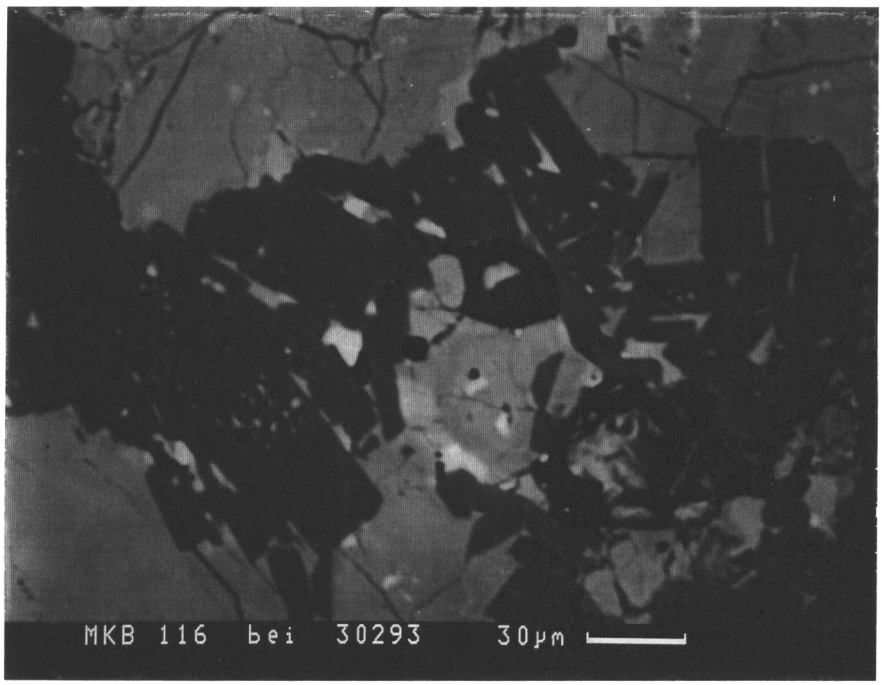

Figure 33. SEM backscattered electron image showing the typical nature of the material on the surface of the refractory brick in the furnace area of one facility.

Coal Ash Studies

One billion tons of coal was consumed in the United States in 1990 to produce electricity, resulting in a concentration of the original non-combustable elements into the 90 million tons of waste created (Sommerlad and Otani, 1991).

The third portion of this study was a cursory examination of samples of slags from a local coal burning power plant in order to allow for comparison of these slags with those examined in the first two parts of this study. At the time of our visit, the small stoker was in operation which moves coal through in thirty minute cycles, burning at temperatures of 800-1000°C. It was operating at the normal summer run conditions of 250 psi. This facility does not collect fly ash. Samples of slag were obtained before water was added to control dust. See Figure 34 for a schematic diagram of a typical coal-burning power plant.

Chen et al. (1986) studied the composition and microstructures of slag produced by the burning of low-grade coals simulated in a research boiler in Canada. The boiler was a pulverized-coal-fired boiler incorporating two tangentially opposed burners. Combustion gases left the furnace at temperatures of 900 to 1100°C.

Bulk Chemistry and Concentration Factors:

The samples studied from the local plant consist of 70% Si-Al-Fe-Ca oxide glass phase and about 30% pyroxene blades, both of fairly consistent composition as can be seen in Table 6. Both the glass and the blades contain Si, Fe, Al, Ti, K, and Ca; however, the Mg and Fe are preferentially concentrated in the blades and the Na is left behind in the glass in all points analyzed.

Table 7 shows the corresponding compositions of the ashes and Table 8 shows the compositions of the slags from Chen's study. As can be seen in these tables, the bulk of the ash and slag is composed of Al, Si, Fe and Ca oxides. The typical composition of the glass matrix found in this study is in Table 6.

Elements originating from the inorganic phases in coals including clays, quartz, carbonates, and sulfides become concentrated 10-15 percent as the result of the combustion of the coal.

Phases and Mineral Analogs:

The samples of slag from the local coal-burning power plant contained approximately 70% Si-Al-Fe-Ca oxide glass and had only one mineral analog present.

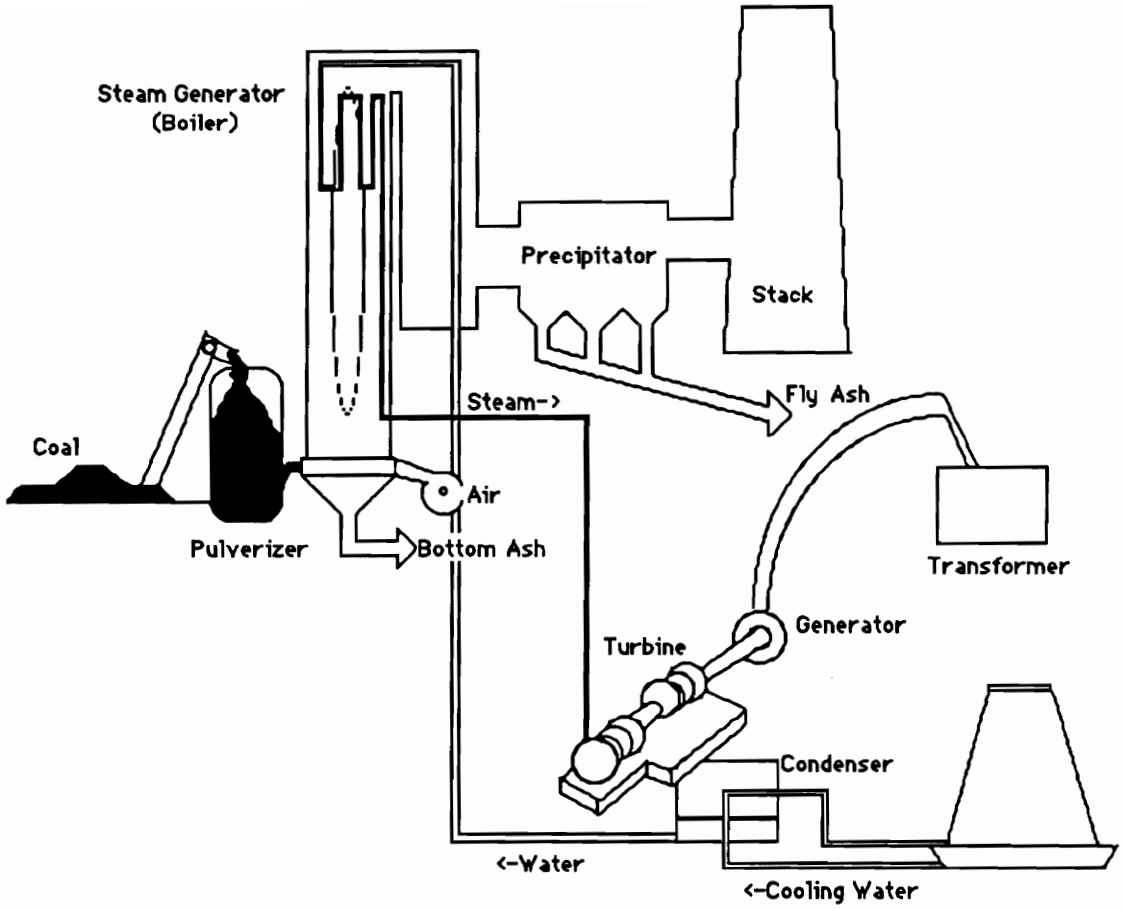

Figure 34. Schematic diagram of a typical coal-burning power plant.

Table 6. Compositions as determined on the SEM of the glass matrix and the blades contained within it from the local coal-burning power plant slag sample are in the first two groups. The last group of data is the average composition of the glass matrix found by Chen et al. (1986) as determined by electron microprobe analysis.

Blades		Glass Matrix		Glass Matrix (Chen)	
Compound	Weight %	Compound	Weight %	Compound	Weight %
SiO_2	52.83	SiO_2	59.58	Al_2O_3	27.4
FeO	23.44	Al_2O_3	23.28	SiO_2	60.4
Al_2O_3	16.11	FeO	6.85	FeO	2.7
MgO	3.63	CaO	6.37	MgO	1.0
TiO_2	1.94	K_2O	1.51	BaO	0.7
K_2O	1.21	Na_2O	1.29	TiO_2	1.6
CaO	0.84	TiO_2	1.11	P_2O_5	0.7
				K_2O	2.4
				CaO	2.9

Table 7. Compositions of the ashes from the coals from Chen et al. (1986). *PST is the potential slagging temperature.

PST*	>1480ºC	1393ºC	1261ºC	1178ºC
Compound	**Weight %**	**Weight %**	**Weight %**	**Weight %**
Al_2O_3	30.2	29.5	20.0	16.7
SiO_2	55.2	56.5	61.5	55.8
Fe_2O_3	1.9	3.0	4.3	5.1
TiO_2	2.1	1.9	0.9	0.6
P_2O_5	1.4	0.8	0.4	0.3
CaO	3.1	2.8	6.0	10.6
MgO	0.4	0.7	1.2	1.4
SO_3	2.0	2.1	3.7	6.4
Na_2O	0.2	0.1	0.3	0.9
K_2O	0.8	1.1	0.9	0.8

Table 8. Compositions of the coal slags from the study by Chen et al. (1986).

(Chen's Numbers ->)	(1)	(2)	(10)	(14)
Compound	**Weight%**	**Weight%**	**Weight%**	**Weight%**
Al_2O_3	30.0	28.7-29.4	20.3-20.5	22.3
SiO_2	59.4	58.3-58.8	66.4-66.9	56.3
Fe_2O_3	2.4	1.5	4.5-4.8	5.6
CaO	2.9	2.5-2.7	4.3-4.6	8.3
MgO	0.8	0.6-0.7	0.9-1.0	1.1
SO_3	<0.1	0.0-0.3	<0.1	1.6
TiO_2	1.4	1.5	0.5	0.9
Na_2O	0.1	0.1	0.2-0.3	0.3
K_2O	1.0	1.0-1.3	0.9	0.6

Always found as blades, pyroxene analogs of Si-Fe-Al-Mg-Ti-K-Ca composition made up as much as 30% of the sample. Pyroxene has the general formula XYZ_2O_6 with Ca^{2+}, Fe^{2+}, Mg^{2+} in the X (or M2) crystallographic site; Fe^{2+}, Mg^{2+}, Fe^{3+}, Al^{3+}, Ti^{4+} in the Y (or M1) site; and Si^{4+} and Al^{3+} in the Z (or tetrahedral) sites. Although Na^{2+} can go into the M2 site, it has been preferentially concentrated in the glass phase.

These findings were consistent with the findings of other researchers.

Textures:

Pyroxene blades were often found aligned, as if they had formed while the glass was still flowing and had not completely solidified, throughout the slag sample from the local power plant. This texture can be seen in Figure 35.

In contrast, Chen et al. (1986) found several textures, as illustrated in his Figures 3-14 (pages 232-234 in his article). Dendritic spinels and iron oxides can be found as seen in his Figures 10 and 13, respectively. Anorthite laths are also common (his Figure 10). Mullite sometimes forms leaf-like clusters as seen in his Figure 8 and quartz was found forming subangular grains (his Figure 7).

Discussion:

As expected from the bulk chemistry of the inorganic phases in coal, the dominant phase found was a Si-Fe-Al oxide glass. The only crystalline mineral analog found was a Fe-Al-Mg pyroxene which crystallized while the temperature in the system was still above the solidus of any other minerals. The glass phase then formed as the slag cooled quickly before any other crystalline phases could develop.

No sulfides were found, despite the fact they were present in the original material. This could be because the S easily goes into a vapor state and is lost from the system.

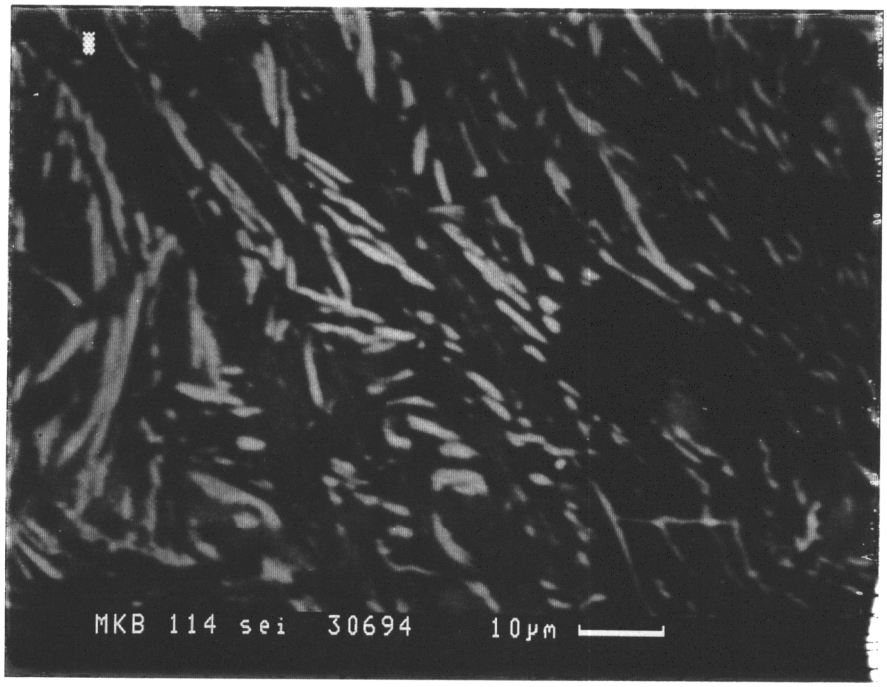

Figure 35. Flow banding of pyroxene blades in glass matrix from the coal ash of a local power plant.

Petroleum Coke Ash/Slag

The slags produced by petroleum coke gasification were not studied in the present study but a brief summary is included here to allow comparison. The description below is abstracted from the work of Groen (1992).

Slags were produced at a Texaco gasification plant similar to the one illustrated in Figure 1. Petroleum coke was ground then mixed with water to form a slurry, similar to that of the coal/sewage sludge mixture. Slag samples for examination and analysis were prepared in a manner similar to that used for the sewage sludge and MSW samples. In addition, Groen prepared some doubly polished thin sections. Groen obtained phase compositions by point analysis on the electron microprobe. Small crystal size made separations difficult; therefore, XRD analysis to confirm phase identifications was not possible.

Bulk Chemistry and Concentration Factors:

Groen (1992) found petroleum coke slags to have V, Ni, S, Fe, Ca, Mg, Si, Al and occasionally Na and K as dominant elements. Slags were divided into three general categories: 1) sulfide dominant, 2) silica dominant, and 3) oxide dominant, which he believed formed in part depending on operational conditions and sample collection timing.

Inorganic phases in the original petroleum have been concentrated as much as 1000 times in the final petroleum coke slags.

Phases and Mineral Analogs:

A wide variety of possible phases were found in Groen's slag categories. Groen noted specifically the abundance of the metal oxides of the spinel family found in these slags (see Groen (1992) for photos of several phase assemblages he found in the petroleum coke gasification slag).

Groen's sulfide dominant slags were found to have only a few sulfide phases, but a host of other phases were present due to the chemical composition of the original petroleum coke. Fe and Ni are the only two metals noted by Groen to commonly form sulfides. Vanadium, although abundant, does not form sulfides, instead going into oxides. Groen noted that sulfide-rich assemblages in this type of slag usually have anhedral matrices of pyrrhotite to troilite to pentlandite to heazlewoodite compositions with inclusions of wustite and free metal.

The silica dominant slags were found by Groen to have only a small number of phases present. This appears to result from the fact that the two most abundant phases are silica-rich glass and spinels, both of which can incorporate a wide variety of elements over large ranges of conditions into their structures.

The third category of slags, the oxide dominant slags, were found to consist mostly of pure, crystalline vanadium oxides and/or mixed crystalline oxides of vanadium with one or more of Fe, Ca, Mg, Ni, Al and Na. Groen only found minor amounts of silica-rich glass and even rarer sulfide grains in this type of slag.

The reader is referred to Groen (1992) for extensive tables of phases found in the petroleum coke slags.

Textures:

Textures found by Groen (1992) varied among the different categories of petroleum coke gasification slags.

Several textures were found by Groen in the sulfide dominant slags as can be seen in his paper. Cruciform free metal crystals and wustite were probably the result of quenching. Free metal inclusions form anhedral blebs, ring "atoll" structures, rounded cruciform skeletal crystals, and blocky euhedral forms which Groen attributed to rapid crystallization or exsolution during cooling. Silica phases were found to form euhedral crystals in the sulfide matrix and in the larger silica-rich glass segregations. Inclusions of spinel vary from euhedral to cruciform, growing directly in the sulfide matrix or silica-rich glass.

Groen found relatively simple textures in the silica dominant slags. He noted the presence of droplets of Fe-Ni sulfide as well as euhedral spinel and silicate crystals in a matrix of amorphous silica-rich glass. Also found were compositional growth zones in spinels and flow features in the glass.

Oxide dominant slags were found to have complex textures similar to those of certain igneous rocks. These textures consisted of euhedral crystalline aggregates of spinels, sesquioxides, and higher vanadium oxides intermixed with droplets of Si-Al-Ca and V-Ca-rich oxide glass in addition to occasional blebs of sulfide (some with oxidation alteration rinds) and oxidation products on earlier-formed spinels.

Reactions with Refractories:

Slags and refractory brick do react with each other to vary degrees depending on such factors as slag chemistry, refractory chemistry, gasification temperature, and the construction of the refractory lining. Al, Cr, Mg and Zr are the most commonly used refractory metals and unexpectedly high concentrations of these elements in slag may result from reaction of the refractory material.

Groen observed considerable reaction with refractory material and discussed its significance.

Comparison of the Four Ash Sources / Conclusions:

Despite differences in bulk chemistries and modes of generation, ashes from fuel production tend to possess many similarities.

Sludge ashes studied were produced in a facility where maximum pressures of the gases approached 900 psi with temperatures near 1315°C. MSW ashes examined were all formed at temperatures around 1000°C and low pressures. Coal ashes were also the result of maximum conditions near 1000°C. Petroleum coke slags studied by other researchers formed under conditions similar to the sludge ashes.

Various bulk chemistries of the ashes can be reviewed in Table 9. The last two columns of this table are for comparison of the ashes to typical bulk chemistries of soil and crustal rocks.

Despite the varied source materials, there was considerable similarity of the products. Overall, the textures and types of mineral analogs found did not vary a great deal from one ash source to the next, as can be seen in previous tables and photos. The greatest variety of phases was found in the MSW ash and petroleum coke slag since the bulk chemistries of the original materials were the most complex. The complexity of the MSW ash came from a complex source, whereas the complexity of the petroleum coke slag resulted after a very high degree of concentration. Even so, many of these phases were variations in composition of one mineral analog family, usually the spinels. The most common phase found in all ashes was an aluminosilicate-rich glass which generally comprised the matrix. This glass phase was found to contain, in addition to Al and Si, some or all of the following elements: Fe, K, Na, Ti, Ca, Mg, P, and Ba. Thus, these elements were locked up in the glasses. The next most widely found phase was spinel which exhibited a wide compositional variation. Spinels, being refractory in nature, tied up the following elements: Fe, Cr, Al, V, Ti, Mn, and rarely Si and Na. The spinels found in the sewage sludge ash contained Fe, Cr, and Al. The spinel type phases found in the MSW ash were predominantly Fe with up to 20 weight percent of Ti, Si, Al, Mg, Ca, Mn, P, Cr, and/or Na oxides. Mineral analogs of olivines and pyroxenes were found in some of the ashes, containing the following elements: Al, Si, Fe, Mn, Mg, and Ca. Ni was found in the petroleum samples as oxides, sulfides, and in alloys with Fe by Groen. Pb and Zn were found as both sulfides (galena and sphalerite, respectively) and in equal amounts as oxides in the sludge ashes. Sulfides were found mostly in the sewage sludge ash and included FeS_2, ZnS, PbS, and $Fe_{1-x}S$. The ZnS and PbS were usually found

Table 9. Overview of the bulk chemistries of the various ashes. The last two columns are average bulk chemistries of soil and crustal rocks. Trace elements shown in ppm.

	Weight Percent				
Species	Sewage Sludge Coarse Slag	MSW	Coal Ash	Soil	Crustal Rocks
SiO_2	46.05	33.4	56.5	41.39	60.22
Al_2O_3	21.74	13.4	29.5	38.2	15.18
(LOI)	----	9.7	----	----	----
CaO	7.72	9.1	----	1.17	5.51
Fe_2O_3	16.15	8.7	3.0	3.47	2.48
Na_2O	0.88	4.2	0.1	1.05	2.99
SO_4	----	3.5	2.5	7.75	2.92
K_2O	1.68	1.7	1.1	1.06	2.86
TiO_2	1.76	1.6	1.9	0.37	0.73
MgO	1.54	1.5	0.7	1.97	3.05
P_2O_5	1.52	1.1	0.8	0.07	0.24
MnO	0.10	0.24	----	0.04	0.14
Totals	99.14	88.14	98.9	96.54	96.32
			ppm		
Zn	560	10000	----	49	70
Cl	----	10400	----	----	600
Pb	900	3800	----	21	14
Cu	960	2000	----	354	60
Ba	990	1100	----	2000	425
B	----	170	----	22	10
Cr	2100	340	----	101	102
Sr	760	220	----	110	370
Cd	----	140	----	0.7	0.15
Sn	----	140	----	2.0	2.3
Ni	710	110	----	75	84
V	----	62	----	56	120
Ag	----	28	----	1.4	0.075
Co	----	18	----	30	25
Se	----	14	----	1.12	0.05
Hg	----	5	----	0.167	0.085
Au	----	0.5	----	0.016	0.004

rimming large grains. Fewer sulfides were found in the MSW ash and included FeS_2 (pyrite) probably because more sulfur was lost in the process and because the more oxidizing environment favored the stability of pyrite. There were only a few elements found as metals. The only free metal found in the sewage sludge ash was Fe in association with both Fe oxides and sulfides. Several free metals were found in the MSW ash, including Fe in association with $Fe_{1-x}S$, Al in association with SiO_2, and Au. The lack of phases bearing volatile elements such as S, Zn, and Pb in the coal and MSW ashes may be due to the fact that these elements were being volatized, either precipitating on the relatively cool walls of the stack or being released into the atmosphere. The completely enclosed gasification process used to process the sewage sludge catches the volatiles.

Phases found by Kirby and Rimstidt (1993) such as carbonates and salts are the most vulnerable to leaching. These are water soluble phases not seen in this thesis work, but which are unquestionably present.

The elements tied up in glasses would generally be considered the next most vulnerable to leaching because the glasses are inherently unstable. Nevertheless, the release of any elements into the environment would be slow and controlled by rates of fluid flow that brings about dissolution.

Metals tied up as sulfides, unless covered by a protective oxidized layer, are also very vulnerable. However, the oxidation of the sulfides would rapidly armor the grains with a layer of oxide or sulfate thereby reducing the rate of dissolution.

Some elements, especially several of the metals about which there is much concern, are in spinels and are held in a well known refractory-type phase which will be much more stable than the glasses. Hence, these spinels will isolate the metals for long periods of time with their release into the environment being very slow. Additionally, the pyroxene-like phases will be more stable than the glasses and will decompose much like natural pyroxenes with slow release of the metals. The free metals are inherently vulnerable to attack, but are readily armored by less soluble oxide coatings.

All types of fuel sources will slowly react with refractory materials, removing Cr and Al from the bricks. However, these elements will then be incorporated into glasses, spinels, or other phases which will react as described above.

REFERENCES

Bawkon, B. 1991: Incineration technologies for managing solid waste: Pollution Engineering, Sept., p.96-102.

Campbell, Tom 1990, a: As garbage mounts, it can't be swept under the carpet: Richmond Times-Dispatch, Aug. 26.

Campbell, Tom 1990, b: Recycling era is ready to roll: Richmond Times-Dispatch, Aug. 27.

Campbell, Tom 1990, c: Incineration plans create split over effects of burning waste: Richmond Times-Dispatch, Aug. 27.

Campbell, Tom 1990, d: Innovation is watchword for our discards in new decade: Richmond Times-Dispatch, Aug. 29.

Carmichael, Robert S. 1989: CRC Practical Handbook of Physical Properties of Rocks and Minerals: CRC Press, Inc., Boca Raton, FL.

Chen, T.T., Quan, D.H.H., Wang, S.S.B. 1986: Compositions and microstructures of furnace-bottom deposits produced from beneficated Western Canadian bituminous coals: Canadian Mineralogist, v. 24, p. 229-237.

Craig, J.C., and Vaughan, D.J. 1981: Ore Microscopy and Ore Petrography: Wiley Interscience, New York, 406 pg.

EPA: Characterization of Municipal Solid Waste in the United States: 1992 Update, Executive Summary: U.S. EPA, July 1992.

From Waste to Energy: Mecklenberg County Engineering Dept.

Groen, J.C. 1992: Microchemical phase characterization of petroleum coke gasification slags: Ph.D. thesis, V.P.I. & S.U., Blacksburg, VA, 182 p.

Kirby, C.S., and Rimstidt, J.D. 1993: Mineralogy and surface properties of municipal solid waste ash: Environmental Science and Technology, v.27, no.4, p.652-660.

Klein, C., and Hurlbut, C.S. Jr., 1977: Manual of Mineralogy 20th Edition: John Wiley & Sons, NY.

Potts, P.J., Tindle, A.G., Webb, P.C. 1992: Geochemical Reference Material Compositions: Whittles Publishing, Boca Raton, FL.

Preston, W.E. 1990: The Texaco coal gasification process: A means to produce clean, cost competitive power from coal: Presented at the A.I.C.E. Spring National Meeting, April 18-22.

Sommerlad, R.E., and Otani, B.T. 1991: Water protection under the clean air act: Pollution Engineering, Sept., p. 85-87.

Steverson, E.M. 1991: Provoking a firestorm: Waste incineration: Environmental Science and Technology, v.25, no.11, p. 1808-1814.

Zang, R.B., and Khan, M.R. 1991: Gasification of sewage sludges: Presentation to the NY Water Pollution Control Assoc.by Texaco Inc., Jan. 15.

APPENDIX A

Table 1. SEM data for sample #1 (sewage sludge) in oxide weight percents.

	Clay Data:		Feldspar Data:
Species	1	2	3
SiO_2	55.36	38.75	62.80
Al_2O_3	28.43	23.47	29.80
K_2O	10.17	5.69	6.86
FeO	2.49	----	----
CaO	1.67	2.80	----
TiO_2	2.32	6.30	----
MgO	0.01	----	----
P_2O_5	----	10.42	----
SO_4	----	11.43	----
Na_2O	----	----	0.01
Totals	99.46	98.86	99.47

Table 2. SEM data for sample #2 (sewage sludge) in oxide weight percents.

Glass compositional data:

Species	1	2	3	4
SiO_2	54.96	43.40	61.45	56.72
Al_2O_3	23.26	15.53	22.66	19.48
FeO	12.86	----	----	17.33
CaO	8.92	----	13.45	6.47
TiO_2	----	----	2.43	----
P_2O_5	----	41.07	----	----
Totals	100.00	100.00	99.99	100.00

Table 3. SEM data for sample #3 (sewage sludge) .

A. Glass compositional data (in oxide weight percents):

Species	1	2	3
SiO_2	62.99	59.38	60.78
Al_2O_3	16.94	24.08	24.56
K_2O	2.81	2.22	4.06
FeO	6.00	7.95	4.57
CaO	3.96	4.75	0.01
TiO_2	1.49	1.62	2.65
P_2O_5	1.98	----	2.64
ZnO	3.84	----	----
Totals	100.01	100.00	99.27

B.Sphalerite compositional data (in weight percents then atomic percents):

Species	1		2		3	
Zn	54.22	39.72	65.33	49.22	64.04	48.17
S	33.05	49.37	30.87	47.42	30.89	47.37
Fe	12.73	10.91	3.80	3.35	5.07	4.46

Table 4. SEM data for sample #4 (sewage sludge) in oxide weight percents.

A. Glass compositional data (corresponds to groundmass 9 in Figure 6):

Species	1
SiO_2	59.26
Al_2O_3	22.67
K_2O	1.42
FeO	4.61
CaO	12.04
Total	100.00

B. Spinel compositional data corresponding to Figure 7:

Species	1	2	3	4	5
CrO	33.58	39.34	34.44	29.79	34.73
FeO	32.81	30.79	31.14	32.41	31.39
Al_2O_3	33.61	29.88	34.41	37.80	33.88
Totals	100.00	100.01	99.99	100.00	100.00

Species	6	7	8
CrO	33.67	42.80	39.39
FeO	31.93	32.51	31.63
Al_2O_3	34.40	24.69	28.98
Totals	100.00	100.00	100.00

Table 5. SEM data for sample #5 (sewage sludge) .

A. Glass compositional data (in oxide weight percents):

Species	1	2
SiO_2	52.28	52.49
Al_2O_3	22.27	22.53
K_2O	1.57	1.54
FeO	12.30	12.28
CaO	7.18	7.37
TiO_2	2.01	1.99
MgO	0.01	<0.01
P_2O_5	1.67	1.59
Totals	99.29	99.80

B. Fe-oxide-rich grain's compositional data (in oxide weight percents):

Species	1
FeO	96.47
CrO	3.22
SO_4	<0.01
Totals	99.70

Table 6. SEM data for sample #6 (sewage sludge) .

A. Glass compositional data (in oxide weight percents):

Species	1	2
SiO_2	57.41	57.37
Al_2O_3	22.86	22.44
FeO	12.39	13.09
CaO	7.34	7.09
Totals	100.00	99.99

B. Compositional data for pyrrhotite grain (weight percent then atomic percent):

Species	1	
Fe	62.77	49.19
S	37.23	50.81

C. Compositional data for the spinel (in oxide weight percents):

Species	1
CrO	56.00
FeO	31.32
Al_2O_3	12.68
Totals	100.00

Table 7. SEM data for sample #7 (sewage sludge) in oxide weight percents.

A. Glass compositional data:

Species	1	2
SiO_2	60.31	58.02
Al_2O_3	21.29	22.36
FeO	10.89	11.84
CaO	7.51	7.78
Totals	100.00	100.00

B. Compositions corresponding to the graph in Figure 10B:

Species	1	2	3	4	5
SiO_2	57.50	63.86	46.48	56.94	53.92
Al_2O_3	22.19	24.10	10.96	27.00	24.93
K_2O	----	2.20	----	----	----
FeO	12.89	----	34.04	6.36	14.82
CaO	7.42	9.84	3.00	9.70	6.33
SO_4	----	----	5.51	----	----
Totals	100.00	100.00	99.99	100.00	100.00

Species	6	7	8	9
SiO_2	49.03	51.68	64.83	58.89
Al_2O_3	24.73	22.68	21.16	24.49
K_2O	----	----	2.43	----
FeO	20.44	10.22	----	8.09
CaO	5.80	15.42	11.58	8.53
MnO	----	----	----	----
SO_4	----	----	----	----
CrO	----	----	----	----
Totals	100.00	100.00	100.00	100.00

Table 8. SEM data for sample #8 (sewage sludge) .

Glass compositional data (in oxide weight percents):

Species	1	2	3
SiO_2	53.65	50.61	53.96
Al_2O_3	28.93	24.23	22.56
K_2O	1.81	1.20	1.74
FeO	8.06	15.73	11.19
CaO	4.25	6.92	6.89
TiO_2	3.28	1.31	1.95
P_2O_5	----	----	1.71
Totals	99.98	100.00	100.00

Table 9. SEM data for sample #9 (sewage sludge) in oxide weight percents.

A. Glass compositional data:

Species	1	2
SiO_2	55.31	47.69
Al_2O_3	21.96	33.78
K_2O	1.39	----
FeO	11.78	12.05
CaO	7.28	6.47
TiO_2	2.28	----
Totals	100.00	99.99

B. Compositions corresponding to graph in Figure 13:

Species	1	2	3	4	5
SiO_2	56.50	56.53	57.29	49.16	56.22
Al_2O_3	21.98	21.83	21.88	26.18	21.98
K_2O	1.46	1.44	1.14	----	1.66
FeO	12.84	13.21	12.36	7.37	12.71
CaO	7.21	6.98	7.33	8.35	7.44
TiO_2	----	----	----	3.61	----
P_2O_5	----	----	----	5.32	----
Totals	99.99	99.99	100.00	99.99	100.01

Species	6	7	8	9
SiO_2	34.47	40.65	36.04	28.01
Al_2O_3	18.09	19.10	21.27	14.32
K_2O	----	----	----	----
FeO	43.45	25.12	20.93	50.84
CaO	2.38	----	5.89	3.77
SO_4	1.61	15.14	10.97	3.06
P_2O_5	----	----	4.90	----
Totals	100.00	100.01	100.00	100.00

Table 10. SEM data for sample #10 (sewage sludge) .

Glass compositional data (in oxide weight percents):

Species	1	2	3
SiO_2	50.51	48.72	51.89
Al_2O_3	18.85	19.95	20.08
K_2O	1.21	----	1.52
FeO	19.09	14.36	13.39
CaO	10.34	16.96	12.36
MgO	----	----	0.01
Totals	100.00	99.99	99.25

Table 11. SEM data for sample #11 (sewage sludge) .

Glass compositional data (in oxide weight percents):

Species	1	2	3
SiO_2	50.48	43.88	54.27
Al_2O_3	21.65	22.85	21.80
K_2O	1.52	----	1.98
FeO	16.45	20.24	15.24
CaO	7.90	10.46	6.71
TiO_2	2.00	2.58	----
Totals	100.00	100.01	100.00

APPENDIX B

Table 1. SEM data of the compositions of the glasses in the MSW ash (in oxide weight percents).

Species	1	2	3	4	5
SiO_2	49.49	56.56	52.85	52.24	47.97
Al_2O_3	1.64	3.22	2.85	4.41	8.11
K_2O	----	1.09	0.76	1.11	1.84
FeO	27.63	26.34	19.30	25.61	17.16
CaO	16.57	----	7.28	----	8.82
MgO	1.28	----	----	----	----
MnO	0.09	----	0.10	----	----
P_2O_5	----	----	0.30	----	----
Na_2O	3.29	12.79	16.55	16.62	16.10
Totals	99.99	100.00	99.99	99.99	100.00

Species	6	7	8	9	10
SiO_2	47.88	62.63	51.75	53.06	49.04
Al_2O_3	7.80	3.57	12.23	6.74	11.30
K_2O	1.66	0.29	----	----	----
FeO	24.59	19.02	10.50	20.57	20.16
CaO	5.98	4.25	16.62	4.74	4.85
TiO_2	----	----	1.64	----	----
MgO	----	----	----	----	----
P_2O_5	1.34	----	----	----	----
Na_2O	10.75	10.24	7.26	14.88	14.65
Totals	100.00	100.00	100.00	99.99	100.00

Species	11	12
SiO_2	64.11	65.57
Al_2O_3	15.41	20.49
K_2O	2.71	1.05
FeO	5.62	2.36
CaO	3.16	3.00
TiO_2	1.43	----
MgO	----	----
P_2O_5	----	----
Na_2O	7.57	7.53
Totals	100.01	100.00

Table 2. SEM data of the compositions of the skeletal spinel-type crystals in the MSW ash (in oxide weight percents).

Species	1	2	3	4	5
SiO_2	----	9.12	5.48	2.99	----
Al_2O_3	----	3.25	3.24	----	----
FeO	30.90	65.75	85.02	94.80	98.48
TiO_2	63.94	20.67	6.26	----	1.52
CaO	----	1.21	----	----	----
MgO	5.16	----	----	----	----
MnO	----	----	----	2.22	----
P_2O_5	----	----	----	----	----
CrO	----	----	----	----	----
Na_2O	----	----	----	----	----
Totals	100.00	100.00	100.00	100.01	100.00

Species	6	7	8	9	10
SiO_2	----	2.27	----	----	----
Al_2O_3	2.69	4.40	3.77	4.30	----
FeO	94.17	70.24	88.28	90.63	99.44
TiO_2	3.14	20.12	----	2.98	----
CrO	----	2.74	----	2.09	----
MgO	----	----	----	----	----
MnO	----	----	----	----	0.43
P_2O_5	----	----	----	----	0.13
V_2O_3	----	0.22	----	----	----
Na_2O	----	----	7.95	----	----
Totals	100.00	99.99	100.00	100.00	100.00

Table 3. SEM data of selected parts of the MSW ash (in oxide weight percents).

A. Glass compositional data:

Species	1
SiO_2	48.12
Al_2O_3	36.70
CaO	15.18
Total	100.00

B. Ilmenite compositional data:

Species	1
FeO	69.55
TiO_2	22.02
MgO	3.85
MnO	4.58
Totals	100.00

C. Spinel compositional data:

Species	1
SiO_2	34.15
TiO_2	39.64
CaO	26.21
Totals	100.00